IFT56 regulates vertebrate developmental patterning by maintaining IFTB integrity and ciliary microtubule architecture.

Daisy Xin[a], Kasey J. Christopher [a], Lewie Zeng[a], Yong Kong[b,c] and Scott D. Weatherbee[a]*

[a]Department of Genetics, Yale University, New Haven, CT 06520

[b]Department of Molecular Biophysics and Biochemistry, Yale University, New Haven, CT 06520

[c]W.M. Keck Foundation Biotechnology Resource Laboratory, Yale University, New Haven, CT 06520

*Corresponding author

scott.weatherbee@yale.edu

Phone: 203-737-1923

Fax: 203-785-4415

Keywords: IFT56; cilia; intraflagellar transport; IFTB; Hedgehog signaling; microtubule structure

SUMMARY STATEMENT

Intraflagellar transport (IFT) is crucial for proper cilia function and is poorly understood. We reveal that IFT56 is key for the integrity and function of IFT and consequently vertebrate development.

ABSTRACT

Cilia are key regulators of animal development and depend on intraflagellar transport (IFT) proteins to form and function, yet the roles of individual IFTs are still unclear. We examined the *Ift56*^{hop} mouse mutant and reveal novel insight into the function of IFT56, a poorly understood IFTB protein. *Ift56*^{hop} mice have normal cilia distribution but display defective cilia structure including abnormal positioning and number of ciliary microtubule doublets. Furthermore, we show that *Ift56*^{hop} cilia are unable to accumulate Gli proteins efficiently, resulting in developmental patterning defects in Shh signaling-dependent tissues such as the limb and neural tube. Strikingly, we further demonstrate that core IFTB proteins are unable to accumulate normally within *Ift56*^{hop} cilia, including IFT88, IFT81, and IFT27, which are critical for key processes such as tubulin transport and Shh-signaling. IFT56 is required specifically for the IFTB complex as IFTA components and proteins that rely on IFTA function are unaffected in *Ift56*^{hop} cilia. These studies define a distinct and novel role for IFT56 in IFTB complex integrity that is crucial for cilia structure and function, and ultimately animal development.

INTRODUCTION

In vertebrates, cilia are essential for many developmental processes including left-right specification, organogenesis, skeleton formation, and neural patterning (Fliegauf et al., 2007; Oh and Katsanis, 2012; Sharma et al., 2008a). As a consequence, defects in cilia formation or function underlie a broad range of human diseases, with varying degrees of severity, collectively referred to as ciliopathies (Badano et al., 2006; Hildebrandt et al., 2011; Lancaster and Gleeson, 2009; Nigg and Raff, 2009; Sharma et al., 2008b; Waters and Beales, 2011). Cilia are near-ubiquitous organelles that extend into the extracellular space and sense mechanical stimuli as well as several signaling molecules (Choksi et al., 2014; Goetz and Anderson, 2010). These include Hedgehog (Hh) ligands, which regulate the development of multiple organ systems including the limb and neural tube (Litingtung and Chiang, 2000; Litingtung et al., 2002). Components of the Hh pathway, including the receptor Patched (Ptch1), the pathway mediator Smoothened (Smo), and Gli transcriptional mediators localize to the cilium and cilia are required for normal Hh pathway activity (Haycraft et al., 2005; Rohatgi et al., 2007). Through a mechanism that is still unclear, the Gli proteins require cilia to form both their functional transcriptional activator (GliA) and repressor (GliR). Without proper cilia formation or function, both positive and negative (ligand-independent GliR) functions of Shh signaling are affected, leading to a range of Hh-related patterning defects in multiple tissues (Liu et al., 2005; May et al., 2005)

In addition to components of the Hh pathway, hundreds of other proteins transit through the cilium via intraflagellar transport (IFT) (Kozminski et al., 1993). This process is mediated by kinesin and dynein microtubule motor proteins, which direct anterograde and retrograde movement respectively (Cole et al., 1998; Pedersen et al., 2008; Rosenbaum and Witman, 2002). Working with the motors are IFT particles, multi-protein complexes that transport proteins involved in cilia formation and function, including tubulin subunits and signaling pathway effectors (Kozminski et al., 1995; Pazour et al., 1998). The IFT particle itself can be biochemically grouped into IFTB and IFTA protein complexes that have distinct functions.

Loss-of-function mutations in most IFTB genes lead to failure of cilia formation due to defects in importing critical cilia-building components, while IFTA mutants form bulbous cilia with proteins accumulating at the distal tip (Blacque et al., 2008; Huangfu et al., 2003; Liem et al., 2012; Qin et al., 2011). This evidence has been interpreted to mean that anterograde trafficking is mediated by IFTB while retrograde transport depends on IFTA function. However, the finding that a subset of IFTB mutants (e.g. *Ift25/27*) retains cilia (Eguether et al., 2014; Keady et al., 2012a) highlights the poorly understood complexity of individual IFT function.

The IFTB complex comprises 16 proteins, and recent studies have begun to dissect the biochemical and structural interactions within the complex (Katoh et al., 2016; Taschner et al., 2014; Taschner et al., 2016). IFT56 (also known as Dyf-13/PIFTC3/Ttc26) is a highly conserved IFTB protein that localizes to flagella/cilia of organisms ranging from the single cell alga *Chlamydomonas reinhardtii* to vertebrates (Blacque et al., 2005; Follit et al., 2009; Franklin and Ullu, 2010; Ishikawa et al., 2014; Zhang et al., 2012). In *C. elegans* and *Chlamydomonas*, disruption of *Ift56* function reduces cilia/flagella length, and zebrafish IFT56 morphants display reduced cilia number (Blacque et al., 2005; Ishikawa et al., 2014). In *Chlamydomonas,* IFT56 associates with motility factors including outer dynein arms, and loss of IFT56 results in a decrease in these proteins leading to impaired motility (Ishikawa et al., 2014). The classic mouse mutant *hop-sterile* (Johnson and Hunt, 1971) was recently reported to harbor a nonsense mutation within *Ift56* (Swiderski et al., 2014). In contrast to *IFT56* mutants in non-mammalian systems, as well as most other IFTB mouse mutants, *Ift56*^{hop} mice are viable and display normal cilia numbers and morphology. This provides a unique opportunity to study IFTB function within intact cilia and suggests distinct roles for IFT56 compared to other IFTB proteins.

Ift56^{hop} mutants are characterized by preaxial polydactyly, gait abnormalities, and male sterility (Johnson and Hunt, 1971). In this study we uncover three key functions of IFT56 in

mammalian primary cilia that explain the developmental defects and shed new light on the roles of IFT56. First, IFT56 is required for the accumulation of Gli2 and Gli3 at the distal tips of cilia. Reduced ciliary Gli2/3 in *Ift56*^{hop} mutants would account for the Shh-dependent limb and neural tube patterning defects observed in *Ift56*^{hop} mutants. Second, while IFT56 is not required to form primary cilia, it is essential for normal microtubule architecture within the ciliary axoneme. *Ift56*^{hop} mouse mutants show a reduced number and abnormal arrangement of ciliary microtubule doublets. Finally, IFT56 is critical for the normal levels and distribution of IFTB proteins, but not IFTA, within cilia. These studies reveal previously undescribed roles of IFT56 as an essential core component of the IFTB complex that is required for the integrity of both IFTB and the cilium structure itself. These results also challenge the current model of IFTB-dependent IFTA transport and demonstrate that IFTA components can undergo intraflagellar transport independently of a complete IFTB particle.

RESULTS

The *hop-sterile* phenotype is caused by a nonsense mutation in *Ift56*

The phenotype of *hop-sterile* homozygotes was suggestive of an underlying defect in cilia formation or function. We used a capture and sequencing approach to test whether the *hop* phenotype was caused by a mutation in a known cilia gene (Johnson and Hunt, 1971). Through exome capture, we identified a cytosine-to-adenosine transversion located at mouse Chr6:38,362,071 in mutants (see Methods). This mutation fell within the coding region of the *Intraflagellar transport 56* (*Ift56*) gene (also known as *TTC26*, *Dyf-13, Piftc3*) (c.1290**C>A**) and was predicted to result in a premature truncation (**Y430X**) of the protein (**Fig. S1**). We confirmed complete linkage between the *hop-sterile* phenotype and the *Ift56* mutation, which has been further corroborated by Bánfi and colleagues (Swiderski et al., 2014).

Ciliary IFT56 is required for induction of Shh targets in the neural tube

Ift56^{hop} mutants were initially described with an abnormal gait (Johnson and Hunt, 1971), which is consistent with a patterning defect in the developing neural tube. As most IFTB mutants lose cilia or form short cilia throughout the embryo including the neural tube, we first tested whether *Ift56*^{hop} mutants showed a similar defect. However, we found that *Ift56*^{hop} mutants are able to form grossly normal cilia both in the neural tube and in culture, at a similar density as controls (**Figs. 1A, S2**). Consistent with Swiderski *et al*., we observe increased cilia length in *Ift56*^{hop} mutants (**Fig. S3**). However, *Ift56*^{hop} mutant cilia lack IFT56 protein (**Fig. 1B**), suggesting potential defects in neural tube cilia function.

In the developing neural tube, Shh forms a ventral gradient of signaling that is transduced primarily through the function of Gli2 activator, with the most ventral cell types requiring the highest level of Shh signaling (Chiang et al., 1996; Ericson et al., 1997; Marti et al., 1995). Cilia function is required in the neural tube to receive the Shh signal (Huangfu et al., 2003). In the rostral neural tube (cervical and forelimb level) of *Ift56*^{hop} embryos, the most ventral cells expressed FoxA2, a high-level target of Shh, similar to controls (**Fig. 1C**). V3 interneuron progenitors, marked by Nkx2.2, are specified by slightly lower levels of Shh and were largely found within their normal domains in *Ift56*^{hop} mutants, dorsal to the floorplate (**Fig. 1D**). However, Nkx2.2 was abnormally expressed in a subset of ventral cells in *Ift56*^{hop} mutants and were mixed with floor plate cells (FoxA2+) at the ventral midline (**Fig. 1D',** arrowheads). Motorneuron progenitors, specified at intermediate levels of Shh signaling, appeared normal in the *Ift56*^{hop} neural tube (**Fig. 1E**). The ventral boundary of Pax6+ neuronal progenitors is limited by Shh signaling, and this restriction was also maintained in *Ift56*^{hop} mutants (**Fig. 1F**). These data indicate a mild effect on rostral neural tube patterning in *Ift56*^{hop} mutants.

Strikingly, we observed differential, but consistent patterning effects of the *Ift56*^{hop} mutation between the rostral and caudal neural tube. Ventral neuronal specification defects were more severe in the caudal neural tube (hindlimb level) of *Ift56*^{hop} embryos compared to rostral regions, with the exception of Pax6, which appeared relatively normal (**Fig. 1J**). FoxA2-positive floor plate cells were almost completely absent (**Fig. 1G** and data not shown) and few V3 interneuron progenitors were specified in caudal regions of *Ift56*^{hop} mutants (**Fig. 1H**). While motorneuron markers maintained their dorsal border, they were additionally expressed throughout the entire ventral half of the *Ift56*^{hop} caudal neural tube (**Fig. 1I**) indicating reduced ventral Shh signaling in the mutants.

IFT56 is essential for Gli-Activator and Gli-Repressor function

Preaxial polydactyly was initially described in *Ift56*^{hop} mutants as an extra digit on the anterior side of the limbs (Johnson and Hunt, 1971). When we examined the developing limbs in more detail, we observed variable expressivity of this trait in *Ift56*^{hop} limbs, ranging from a thickening of digit 1 to a complete ectopic digit, including duplicated meta-carpals and –tarsal elements. In the mutant forelimbs, the ectopic digit always displayed digit 1 identity (i.e. 2 phalanges; **Fig. 2A**). However, ectopic hindlimb digits occasionally adopted a more posterior identity (i.e. 3 phalanges; 25%, n=5/20 hindlimbs; **Fig. 2B** and data not shown).

Shh signaling regulates digit number and identity through the function of GliA in the posterior, and a ligand-independent GliR function in the anterior (Bowers et al., 2012; Chiang et al., 2001; Litingtung et al., 2002; te Welscher et al., 2002; Wang et al., 2007). Ectopic Shh expression in the anterior limb has been reported in multiple cases of preaxial polydactyly in mice, cats, dogs and humans (Gurnett et al., 2007; Lettice, 2003; Park et al., 2008; Sharpe et al., 1999; Sun et al., 2008). However, preaxial polydactyly can also develop in the absence of ectopic Shh, as observed in cilia mutants (Christopher et al., 2012; Haycraft et al., 2005; Liu et al., 2005; Weatherbee et al., 2009). This is thought to be due to the disruption of both GliA and GliR function as a result of cilia loss or dysfunction (Haycraft et

al., 2005; Liu et al., 2005). In *Ift56*^{hop} limbs, similar to the neural tube, normal numbers of cilia form but they lack the IFT56 protein (**Fig. 2C**). This raised the question of whether loss of IFT56 in limb cilia alters expression of Shh or affects downstream components of the pathway.

We found that *Shh* transcripts were expressed in a comparable domain in *Ift56*^{hop} mutant and control limb buds, indicating that the preaxial polydactyly was not due to ectopic anterior *Shh* expression (**Fig. 2D**). To test whether GliA function was disrupted, we examined *Gli1*, a direct positive target of Shh signaling (Liu et al., 2005). The *Gli1* expression domain was largely normal in *Ift56*^{hop} limb buds (**Fig. 2E**), in contrast to several IFTB mutants which lose *Gli1* expression completely despite normal *Shh* expression (Liu et al., 2005). We also assessed *Gli1* transcript levels quantitatively, and while they were decreased in mutants compared to controls, this reduction did not reach significance (**Fig. S4**). To test GliR function, we examined the expression of *Gremlin1* (*Grem1*), which is induced by GliA activity in the posterior limb bud and repressed by GliR function in the anterior limb (Vokes et al., 2008). The posterior domain of *Grem1* expression was slightly reduced in mutants, consistent with Gli1 reduction, but more strikingly, we consistently observed ectopic expansion of *Grem1* in the anterior limb (**Fig. 2F**). Together these data indicate that reduced GliR function, rather than ectopic Shh pathway activation likely underlies preaxial polydactyly in *Ift56*^{hop} limbs.

Ciliary accumulation of Gli proteins is reduced in *Ift56*^{hop} tissues

Our analyses of *Ift56*^{hop} mutant neural tubes and limbs indicate that IFT56 is critical for both GliA and GliR function, similar to other IFTB mutants, although the *Ift56*^{hop} phenotype is milder. Unlike most IFTB mutants, *Ift56*^{hop} animals form normal numbers of cilia, which may account for the milder phenotype, but also suggests that abnormal Gli activity is not due to cilia loss but rather defective cilia function. Thus, we examined mouse embryonic fibroblasts (MEF) cilia to better understand how the *Ift56*^{hop} mutation affected the Shh pathway. Smo

accumulates in cilia in the presence of the Hh ligand or a Smoothened agonist (SAG), and we discovered that the distribution and intensity of ciliary Smo was unaffected in *Ift56*^{hop} cilia when the Hh pathway is activated (**Fig. 3A,B**). Gli proteins normally accumulate at the distal tips of cilia in response to Hh pathway activation. Strikingly, Gli2 and Gli3 ciliary tip accumulation was significantly reduced in *Ift56*^{hop} cilia, and a large percentage of mutant cilia showed no detectable Gli2/3 localization (**Fig. 3C-F**). To test the physiological relevance of this finding, we also examined Gli2 in *Ift56*^{hop} cilia, both in the caudal (hindlimb region) neural tube epithelium and in limb mesenchyme. Throughout the posterior limb, few cilia had strong accumulation of Gli2 in *Ift56*^{hop} mutants, and most exhibited low or no levels of Gli2 within cilia. (**Fig. 3G-I**). We similarly observed fainter Gli2 in the neural tube cilia of *Ift56*^{hop} mutants overall (**Fig. S5**). These data show that although cilia form in *Ift56*^{hop} mutants, IFT56 is required for the proper accumulation of ciliary Gli proteins during development.

IFT56 is required for the integrity of the IFTB complex in cilia

Movement of cargo such as Gli proteins and ciliary subunits into and out of the cilium requires the function of IFT complexes (Follit et al., 2009). While IFT56 is a known component of the IFTB complex, its role in primary cilia was unclear. We began by examining IFT localization to better understand the effect on IFT complex integrity and function when IFT56 is disrupted. Surprisingly, we discovered that in *Ift56*^{hop} MEFs, while the amount of IFT88 along the length of the ciliary axoneme was not significantly altered, IFT88 accumulated at the proximal base of cilia in *Ift56*^{hop} MEFs (**Fig. 4A,B**). As IFT88 is critical for cilia formation, this result was unexpected and prompted us to further examine whether additional IFT components required IFT56 for their ciliary localization.

Recent studies have begun to dissect out distinct roles of IFTB proteins within the complex. For example, in contrast to IFT88, IFT81 and IFT74 serve as a “tubulin module” that binds and transports tubulin within cilia (Bhogaraju et al., 2013). IFT25 and IFT27 act as a “Shh module” and are important in localizing Shh signaling components within cilia (Eguether et al., 2014; Keady et al., 2012b; Liew et al., 2014). Similar to IFT88, we observed pooling of

IFT81 at the *Ift56*^{hop} ciliary base. Additionally, we discovered a significant reduction of IFT81 protein in the axoneme in *Ift56*^{hop} cells (**Fig. 4C,D**). Unlike IFT88 and IFT81, IFT27 did not pool at the base of mutant cilia, but was dramatically decreased in *Ift56*^{hop} axonemes (**Fig. 4E,F**). To test whether this was physiologically relevant, we examined limb mesenchyme cilia *in vivo* and confirmed a strong and significant reduction of both IFT81 and IFT27 in *Ift56*^{hop} mutants (**Fig. 4G-L**). Similar to our MEF studies, IFT27 was significantly reduced in limb *Ift56*^{hop} mesenchyme cilia (**Fig. 4J-L**). However, IFT81 showed a stronger phenotype *in vivo* compared to MEFs and was significantly reduced throughout the entire *Ift56*^{hop} ciliary axoneme (**Fig. 4G-I**). This could suggest different requirements for IFT56 within cilia of distinct tissues. Together, these data indicate a key role for IFT56 in the ciliary localization of other IFTB components. In particular, the strong reduction in IFT27 could explain the Shh-related cilia defects that lead to subsequent developmental patterning abnormalities in *Ift56*^{hop} mutants.

The *Ift56*^{hop} mutation disrupts ciliary microtubule architecture

One crucial function of IFT proteins is transporting components required to build the cilium, and at least three IFTs appear to be involved in ciliary tubulin transport (Bhogaraju et al., 2013; Taschner et al., 2016), including IFT81, which we observed pooling at the base of *Ift56*^{hop} cilia. We used transmission electron microscopy (TEM) to examine *Ift56*^{hop} neural tube cilia for potential defects in the structure of the cilium. Consistent with normal cilia numbers in *Ift56*^{hop} mutants, basal bodies appeared to dock normally at the apical side of cells lining the neural tube (**Fig. 5A,B**). Sections through the basal bodies further showed the typical 9+0 ring of microtubule triplets in both mutants and controls (**Fig. 5C,D**). However, while the axoneme of control primary cilia contain a 9+0 ring of microtubule doublets (**Fig. 5E**), *Ift56*^{hop} cilia frequently displayed disorganized structures including abnormal positioning and number (ex. 8+0, 7+0) of the microtubule doublets (**Fig. 5F-H**). These misalignments and tubule losses were never observed in control cilia. These data demonstrate that IFT56 is

essential for proper microtubule organization within the ciliary axoneme, which may be linked to defects in IFT81 localization (**Fig. 4C**).

IFT56 is not required for IFTA localization or function

Ciliary cargo transport is carried out by the combined actions of IFTB and IFTA that together form the IFT particles. To test whether the IFTB defects observed in *Ift56*^{hop} cilia (**Fig. 4**) in turn affected ciliary transport of the IFTA complex, we analyzed the localization of two core IFTA proteins, IFT140 and IFT122. We were surprised to find that both IFT140 and IFT122 protein levels and localization were normal in *Ift56*^{hop} cilia (**Fig. 6A-D**). To verify that IFTAs were functioning normally in *Ift56*^{hop} cilia, we examined several proteins that depend upon IFTA for ciliary localization (Liem et al., 2012; Qin et al., 2011). Adenylyl Cyclase III (AC3) is involved in determining cilia length (Ou et al., 2009; Wang et al., 2011), and was present at normal levels in *Ift56*^{hop} cilia (**Fig. 6E**). Polycystin2 (PC2) is a calcium channel required for mechanosensation (Cai et al., 1999), and Arl13b is a small GTPase required for normal ciliary ultrastructure and Shh signaling (Caspary et al., 2007), and both of these proteins localized normally in *Ift56*^{hop} cilia (**Fig. 6F,G**). These results demonstrate that IFT56 is dispensable for IFTA localization and function but instead is specifically required for IFTB complex integrity and ciliary trafficking.

DISCUSSION

The IFT complex consists of 16 IFTB proteins and 6 IFTA proteins, which together are critical for the formation, maintenance and signaling properties of cilia. Recent studies uncovered key biochemical and structural details of protein-protein interactions within the IFTB subcomplex (Katoh et al., 2016; Taschner et al., 2014; Taschner et al., 2016), yet the functional roles of individual IFTBs within cilia are still being elucidated. Defining the specific requirements of IFTB proteins in cilia has been particularly difficult as most IFTB mutants lack cilia altogether, precluding efforts to study their roles in protein trafficking and cilia

maintenance. Using the *Ift56*^{hop} mutant, which exhibits ciliopathic phenotypes but retains its cilia, we uncovered several distinct roles for IFT56 in the integrity of IFTB and trafficking of Shh signaling proteins, as well as the microtubule organization of mammalian primary cilia.

IFTB is compartmentalized into a stable core known as IFTB-1 (comprising IFTs 88, 81, 74, 70, 52, 46, 27, 25, 22), and a second subcomplex known as IFTB-2 (IFTs 172, 80, 57, 54, 38, 20) (Taschner et al., 2016). IFT56 is one of the least studied IFTB proteins in vertebrates, but was shown to interact directly with IFT46 via Yeast-2-hybrid (Swiderski et al., 2014), suggesting it is part of IFTB-1. Biochemical analysis of *Chlamydomonas IFT56* mutant flagella showed depletion of motility proteins and dynein outer arms, suggesting that IFT56 is primarily required to traffic motility factors into cilia/flagella (Ishikawa et al., 2014). However, *Ift56*^{hop} animals have clear defects in immotile primary cilia, and in the present study, we demonstrate that IFT56 is also required for protein trafficking in primary cilia; specifically for the entry of distinct IFTB components. Depending on tissue type, the loss of ciliary IFT56 can lead to pooling of specific IFTBs (IFT88, 81) at the proximal base of embryonic fibroblast cilia while in limb mesenchyme cilia, the same IFTs are reduced throughout the axoneme. It is likely that IFT56 and/or other IFTs have varied functions within the IFT particle in different tissue systems. Overall, our data suggest that IFT56 is essential in maintaining IFTB complex integrity in mammalian primary cilia, and that loss of ciliary IFT56 may affect a subset of the complex (IFT27) more strongly than others (IFT88, 81), depending on tissue type.

Despite the abnormal localization of IFTB proteins, the IFTB complex retains enough function in *Ift56*^{hop} mutants to form cilia, although the cilia that do form cannot transduce Shh signaling effectively. We observed defective Gli2 accumulation at *Ift56*^{hop} cilia tips both *in vitro* and *in vivo*, and others have reported decreased responsiveness of a Gli-reporter gene expression during Shh induction (Swiderski et al., 2014), indicating that the reduction in Gli2 accumulation affects downstream Shh signaling. This defect in Gli2 accumulation is likely

due to the strong reduction in ciliary IFT27. Recent evidence suggests that IFT27/25 promotes transport of ciliary Smo and Ptch1 through a BBSome-dependent mechanism (Eguether et al., 2014; Keady et al., 2012a; Liew et al., 2014). However, there is little evidence for whether or how Glis are transported by IFTs. IFT mutants lack or have short cilia, further complicating experiments to examine how Glis function in cilia without efficient protein transport. Here, we find that loss of ciliary IFT56 and improper localization of a subset of IFTBs, including IFT27, directly affects Gli accumulation at cilia tips independently of Smo transport. This suggests that individual IFTBs affect cilia-dependent Shh signaling through different mechanisms, where IFT27/25 is important for Smo transport, and IFT56 is crucial for Gli accumulation. Whether the loss of other IFTs from cilia affects localization of signaling function similarly remains to be determined.

One surprise from our study is that core IFTA proteins (IFT122, 140) localized normally in *Ift56*^{hop} mutant cilia despite defects in ciliary IFTB. Ciliary membrane and associated proteins including Smo, Arl13b, AC3, and PC2, which have been shown to depend on ciliary IFTA (Liem et al., 2012) also localize normally, further suggest that IFTA is functioning in the absence of IFT56 and the complete IFTB particle. This is unexpected, as IFTA proteins have long been thought to enter cilia together with IFTB proteins through the function of kinesin-2 (Blacque et al., 2008; Hsiao et al., 2012). In mice, most IFTB and kinesin-2 mutants lose cilia (Berbari et al., 2011; Botilde et al., 2013; Houde et al., 2006; Huangfu et al., 2003; Lee et al., 2015; Marszalek et al., 1999), suggesting that IFTB and kinesin-2 are crucial for anterograde transport of cilia proteins and ciliogenesis. IFTA and dynein mouse mutants have short, bulbous cilia that accumulate IFTs (Cortellino et al., 2009; May et al., 2005; Mill et al., 2011; Qin et al., 2011; Tran et al., 2008), implicating a role in retrograde transport and the recycling of ciliary proteins. However, distinct exceptions including IFT56, 27, 25 (IFTB) mutants (Eguether et al., 2014; Keady et al., 2012a; Swiderski et al., 2014) provide evidence suggesting that IFTB and IFTA may not be restricted to anterograde and retrograde trafficking respectively. Our data suggests that IFTA can enter cilia and function properly

despite the loss and reduction of several IFTB proteins, and does not depend on the complete IFTB particle. Instead, individual IFTB proteins have differential roles within the complex, some of which may be crucial for IFTA transport and others for ciliary cargo. Rather than attributing specific transport roles to each complex, is more likely that IFT acts as one unit that travel throughout the cilium by interacting either directly or indirectly with kinesin and dynein motors, and individual IFT proteins have distinct and specific functions within ciliary protein transport and subsequent vertebrate development.

In addition to defects in signaling, *Ift56*^{hop} primary cilia also exhibited microtubule doublet loss and misalignment, similar to abnormalities originally described in *Ift56*^{hop} sperm tail flagella (Johnson and Hunt, 1971). This suggests there may be global cilia structural defects in *Ift56*^{hop} mutants. We also observed a strong reduction of IFT81 in *Ift56*^{hop} cilia, one of the IFTBs with tubulin-binding capabilities (Bhogaraju et al., 2013; Taschner et al., 2016). The abnormal IFT81 localization to *Ift56*^{hop} cilia may explain the microtubule defects. However, it is unclear at this point whether the primary defect is the inability of microtubules to build or maintain proper cilia structure during ciliogenesis and thus disrupt IFTB localization, or if loss of IFT56 affects IFT integrity and potentially other cargo to disrupt cilia ultrastructure. Interestingly, we did not observe microtubule defects at the basal body level (microtubule triplets), suggesting that the cilium begins to form normally and is unable to continue at the axonemal level, or is unable to be maintained properly.

Despite reduced Shh signaling functions, cilia structure abnormalities, and key IFTB localization defects, the *Ift56*^{hop} phenotype is fairly mild compared to most IFTB mutants, which display severe defects including neonatal lethality, left-right defects, and cyst formation (Berbari et al., 2011; Botilde et al., 2013; Eguether et al., 2014; Huangfu et al., 2003; Keady et al., 2012b). Intriguingly, studies in *Chlamydomonas* show that while IFT56 mutants lose the distal tips of flagella and flagellar motility, mutant flagella did not display changes in IFT rates, suggesting that IFT56 is not essential for IFT movement within cilia

(Ishikawa et al., 2014). This is different from most other IFTB mutants that lack the IFT process altogether and thus lose cilia completely. Instead, these studies, along with our data suggest that IFT56 has a specific role within IFTB that promotes complex integrity and either indirectly or directly affects cargo transport, but is less crucial in ciliogenesis and the IFT process overall.

Recently, independent of our studies, Bánfi and colleagues isolated the *Ift56*^{hop} mutation via standard meiotic recombination mapping (Swiderski et al., 2014). Similar to our findings, they found that the *Ift56*^{hop} phenotype results from reduced Shh signaling; however, Bánfi and colleagues reported no significant changes in Gli2 and Gli3 accumulation in *Ift56*^{hop} cilia or changes in Gli protein levels. This contrasts with our studies, which found reduced Gli2/3 accumulation following pathway activation (SAG treatment) in MEFs. One possible explanation for this discrepancy is differences in experimental conditions between the studies, including amounts and duration of Hh pathway activation. Our *in vivo* studies showing that Gli2 is reduced in *Ift56*^{hop} mutant cilia in both the limb and neural tube argues that our cell culture parameters more accurately reflect the situation in the embryo. Our data further suggest that the defects in ciliary accumulation of Glis and reduction in Shh signaling are likely secondary effects of abnormal IFTB trafficking and cilia function.

Long overlooked, cilia research has recently emerged as essential both for understanding developmental pathways in many animals as well as deciphering human disease. An increasing number of human diseases (ex. Nephronophthisis, Jeune's Asphyxiating Thoracic Dystrophy, COACH) and syndromes (ex. Joubert, Bardet-Biedl, Oral-Facial-Digital type 1, Meckel) have been linked to abnormal development, morphology, or function of the cilium (Badano et al., 2006; Lancaster and Gleeson, 2009; Nigg and Raff, 2009; Sharma et al., 2008b; Waters and Beales, 2011). Given the breadth and severity of cilia-associated defects, elucidating the genetics of ciliopathies is essential to our understanding of how cilia impact development and human health. Our identification of IFT56 as a key regulator of

IFTB ciliary localization and function further sheds light on the distinct mechanisms of intraflagellar transport and its importance in cilia function.

MATERIALS AND METHODS

Mouse strains

Mouse experiments were performed in accordance with the Yale Institutional Animal Care and Use Committee guidelines. The *hop-sterile* (*hop*) strain was obtained from The Jackson Laboratory. All analyses in this manuscript were performed on the BALB/cByJ background, with the exception of skeletal preparations, which were analyzed on an F1 C57BL/6J-BALB/cByJ intercross background. Mice of both sexes were used and adult animals were maintained until approximately 1-1.5 years of age. Ages of animals used in experiments ranged from e10.5 to e18.5.

Exome sequencing of *hop*

Genomic DNA from a *hop* homozygote and BALB/cByJ control was obtained from the Jackson Laboratory's DNA Resource. Exomes were captured at the Yale Center for Genome Analysis, using the NimbleGen SeqCap EZ Mouse Exome, following NimbleGen protocols. Captured pools were sequenced (75bp, paired-end) on an Illumina HiSeq 2000 using previously described methods (Choi et al., 2009). We obtained ~91 million (BALB/cByJ) to ~113 million (*hop*) high-quality reads.

Illumina reads were first trimmed based on their quality scores to remove low-quality regions using the program Btrim (Kong, 2011). A cutoff of 20 for average quality scores within a moving window of size 5-bp was used. Minimum acceptable read length was 25-bp. Other parameters of Btrim were set to defaults. The pre-processed reads were then aligned to the mouse genome reference sequence (mm9) using the BWA mapping program (Li et al., 2009). The mapping results were converted into SAMtools pileup format using SAMtools programs (Li et al., 2009). PCR duplicates were removed using the rmdup command from

SAMtools, resulting in ~84x (BALB/cByJ) or ~100x (*hop*) coverage across the exome. >97% of all bases included in the exome showed at least 8x coverage and >90% of the bases showed at least 20x coverage.

Mutation analysis

Single nucleotide variations (SNVs) were called using SAMtools' pileup command. Further filtering was performed using in-house scripts to exclude those SNV calls that had less than 3 reads or a SNP score less than 20. Annotation was added based on the UCSC RefSeq gene model (Pruitt et al., 2009). To identify homozygous mutations, set the filters to exclude any mutations with a major allele frequency <90%. We scanned the genome using a 100Kb sliding window to identify regions with homozygous single nucleotide polymorphisms (SNPs). This provided us with unbiased mapping data, and resulted in a list of potential causative mutations. The list of SNPs was then filtered for known SNPs (dbSNP build 128) and repeat elements.

Skeletal staining and Expression Analysis

Skeletons were prepared and stained with Alcian blue and Alizarin red using standard methods (Nagy, 2003). *in situ* hybridizations and immunofluorescence analyses were performed using standard methods (Nagy, 2003).

Transmission Electron Microscopy

e11.5 embryos were dissected in ice cold 4% paraformaldehyde (PFA). A transverse cut was made between the fore- and hindlimbs, and the caudal portion of each sample was fixed with 2% PFA and 2.5% glutaraldehyde in 0.1 M sodium cacodylate buffer for 30 minutes at room temperature, followed by an additional hour at 4°C. Embryos were washed three times in sodium cacodylate buffer at 4°C, and then processed for TEM according to standard procedures by the Yale Center for Cellular and Molecular Imaging.

Primary Antibodies

Monoclonal antibodies that recognize Pax6, Nkx6.1, and Nkx2.2. were obtained from the Developmental Studies Hybridoma Bank developed under the auspices of the NICHD and maintained by the Department of Biological Sciences, The University of Iowa (Iowa City, IA, USA). Additional antibodies used included Olig2 (Millipore, Billerica, MA, USA), acetylated α-tubulin and γ-tubulin (Sigma-Aldrich, St. Louis, MO, USA), IFT56 (Novus Biologicals, Littleton, CO, USA), FoxA2 (Abcam), ACIII (Santa Cruz), PC2 (gift from Stefan Somlo), Arl13b (gift from Tamara Caspary), Gli2 and IFT122 (gift from Jonathan Eggenschwiler), Gli3 (gift from Suzie Scales), IFT81 and IFT88 (Proteintech), IFT27 and IFT140 (gift from Greg Pazour). See Supplemental Materials and Methods for additional details.

Cell Culture and immunostaining

Mouse embryonic fibroblasts (MEFs) were derived using standard methods (Nagy et al., 2002) and maintained in a mix of DMEM (1x hi-glucose, Gibco) + 10% fetal bovine serum (FBS, Atlanta Biologicals). For cilia staining, cells were plated on coverslips, grown to confluence, and starved for 48-72 hours in DMEM containing 0.5% FBS. Cells on coverslips were fixed with 2% PFA for 20 min at room temperature followed by 100% MeOH for 5 min at room temperature, and then blocked with 1% goat serum and 0.1% Triton X-100 in PBS for 1 hour at room temperature. Primary antibody in blocking serum was added and incubated overnight at 4C. Secondary antibody in blocking serum was added for 2 hours at room temperature. Samples were mounted on slides (Denville) using Vectashield (Vector Laboratories, Inc). For cells subjected to SAG treatment, 0.1mM SAG was added for 8 hours after 48 hours of cell starvation. All experiments involving MEFs were replicated on at least 3 animals of the same genotype.

Imaging and image analysis

Skeletal stainings were imaged on a Zeiss SteREO Discovery microscope; neural tube and MEF cilia stainings (ACIII, Arl13b, PC2, stable cell lines) were imaged on a Zeiss Axiovert using Carl Zeiss AxioVision Product Suite. Gli2, Gli3, IFT81, 88, 27, 140, 122 (MEFs and tissue) samples were imaged with a Leica SP5 inverted confocal microscope using Leica Application Software. At least 20 cilia in 3 or more sections were imaged per slide, and biological and technical replicates were performed at least 3 times each. Image analysis was performed in ImageJ. To compare intensity of Gli and IFT markers in MEF cilia, integrated density values were generated for individual axonemes by selecting the entire cilium as marked by acetylated α-tubulin, and normalized to cilia length. The same analyses were performed for cilia *in vivo*, but Arl13b was used to mark the cilium. Tip and base intensity measurements were performed similarly, but with a fixed rectangular selection at the tip and base of individual cilia across multiple samples. Two-tailed Student's T-tests were performed in Excel to compare 2 groups and determine significance.

ACKNOWLEDGEMENTS

We would like to thank Anita Fernandez, Karel Liem, Emilie Legue, and members of the Weatherbee lab for discussions and feedback on the manuscript, as well as Greg Pazour, Jonathan Eggenschwiler, Suzie Scales, Tamara Caspary, and Stefan Somlo for antibodies.

COMPETING INTERESTS

The authors declare no competing or financial interests.

AUTHOR CONTRIBUTIONS

All authors performed some of the experiments. YK analyzed the exome data. DX and SDW prepared and edited the manuscript.

FUNDING

This publication was made possible by Grants R01AR059687 from NIAMS/NIH, P30DK090744 from NIDDK/NIH, training grant T32GM007499 from NIGMS/NIH, and training grant T32HD007149 from NICHD/NIH, and a National Science Foundation Graduate Research Fellowship under DGE-0644492 (KJC). Its contents are solely the responsibility of the authors and do not necessarily represent the official views of the NIH or NSF.

REFERENCES

Badano, J. L., Mitsuma, N., Beales, P. L. and Katsanis, N. (2006). The ciliopathies: an emerging class of human genetic disorders. *Annual review of genomics and human genetics* **7**, 125-148.

Berbari, N. F., Kin, N. W., Sharma, N., Michaud, E. J., Kesterson, R. A. and Yoder, B. K. (2011). Mutations in Traf3ip1 reveal defects in ciliogenesis, embryonic development, and altered cell size regulation. *Developmental biology* **360**, 66-76.

Bhogaraju, S., Cajanek, L., Fort, C., Blisnick, T., Weber, K., Taschner, M., Mizuno, N., Lamla, S., Bastin, P., Nigg, E. A., et al. (2013). Molecular basis of tubulin transport within the cilium by IFT74 and IFT81. *Science* **341**, 1009-1012.

Blacque, O. E., Cevik, S. and Kaplan, O. I. (2008). Intraflagellar transport: from molecular characterisation to mechanism. *Frontiers in bioscience : a journal and virtual library* **13**, 2633-2652.

Blacque, O. E., Perens, E. A., Boroevich, K. A., Inglis, P. N., Li, C., Warner, A., Khattra, J., Holt, R. A., Ou, G., Mah, A. K., et al. (2005). Functional genomics of the cilium, a sensory organelle. *Current biology : CB* **15**, 935-941.

Botilde, Y., Yoshiba, S., Shinohara, K., Hasegawa, T., Nishimura, H., Shiratori, H. and Hamada, H. (2013). Cluap1 localizes preferentially to the base and tip of cilia and is required for ciliogenesis in the mouse embryo. *Developmental biology* **381**, 203-212.

Bowers, M., Eng, L., Lao, Z., Turnbull, R. K., Bao, X., Riedel, E., Mackem, S. and Joyner, A. L. (2012). Limb anterior-posterior polarity integrates activator and repressor functions of GLI2 as well as GLI3. *Developmental biology* **370**, 110-124.

Cai, Y., Maeda, Y., Cedzich, A., Torres, V. E., Wu, G., Hayashi, T., Mochizuki, T., Park, J. H., Witzgall, R. and Somlo, S. (1999). Identification and Characterization of Polycystin-2, the PKD2 Gene Product. *Journal of Biological Chemistry* **274**, 28557-28565.

Caspary, T., Larkins, C. E. and Anderson, K. V. (2007). The graded response to Sonic Hedgehog depends on cilia architecture. *Developmental cell* **12**, 767-778.

Chiang, C., Litingtung, Y., Harris, M. P., Simandl, B. K., Li, Y., Beachy, P. A. and Fallon, J. F. (2001). Manifestation of the limb prepattern: limb development in the absence of sonic hedgehog function. *Developmental biology* **236**, 421-435.

Chiang, C., Litingtung, Y., Lee, E., Young, K. E., Corden, J. L., Westphal, H. and Beachy, P. A. (1996). Cyclopia and defective axial patterning in mice lacking Sonic hedgehog gene function. *Nature* **383**, 407-413.

Choi, M., Scholl, U. I., Ji, W. Z., Liu, T. W., Tikhonova, I. R., Zumbo, P., Nayir, A., Bakkaloglu, A., Ozen, S., Sanjad, S., et al. (2009). Genetic diagnosis by whole exome capture and massively parallel DNA sequencing. *Proceedings of the National Academy of Sciences of the United States of America* **106**, 19096-19101.

Choksi, S. P., Lauter, G., Swoboda, P. and Roy, S. (2014). Switching on cilia: transcriptional networks regulating ciliogenesis. *Development (Cambridge, England)* **141**, 1427-1441.

Christopher, K. J., Wang, B., Kong, Y. and Weatherbee, S. D. (2012). Forward genetics uncovers Transmembrane protein 107 as a novel factor required for ciliogenesis and Sonic hedgehog signaling. *Developmental biology* **368**, 382-392.

Cole, D. G., Diener, D. R., Himelblau, A. L., Beech, P. L., Fuster, J. C. and Rosenbaum, J. L. (1998). Chlamydomonas Kinesin-II–dependent Intraflagellar Transport (IFT): IFT Particles Contain Proteins Required for Ciliary Assembly in Caenorhabditis elegans Sensory Neurons. *The Journal of cell biology* **141**, 993-1008.

Cortellino, S., Wang, C., Wang, B., Bassi, M. R., Caretti, E., Champeval, D., Calmont, A., Jarnik, M., Burch, J., Zaret, K. S., et al. (2009). Defective ciliogenesis, embryonic lethality and severe impairment of the Sonic Hedgehog pathway caused by inactivation of the mouse complex A intraflagellar transport gene Ift122/Wdr10, partially overlapping with the DNA repair gene Med1/Mbd4. *Developmental biology* **325**, 225-237.

Eguether, T., San Agustin, J. T., Keady, B. T., Jonassen, J. A., Liang, Y., Francis, R., Tobita, K., Johnson, C. A., Abdelhamed, Z. A., Lo, C. W., et al. (2014). IFT27 Links the BBSome to IFT for Maintenance of the Ciliary Signaling Compartment. *Developmental cell* **31**, 279-290.

Ericson, J., Briscoe, J., Rashbass, P., van Heyningen, V. and Jessell, T. M. (1997). Graded sonic hedgehog signaling and the specification of cell fate in the ventral neural tube. *Cold Spring Harbor symposia on quantitative biology* **62**, 451-466.

Fliegauf, M., Benzing, T. and Omran, H. (2007). When cilia go bad: cilia defects and ciliopathies. *Nature reviews. Molecular cell biology* **8**, 880-893.

Follit, J. A., Xu, F., Keady, B. T. and Pazour, G. J. (2009). Characterization of mouse IFT complex B. *Cell motility and the cytoskeleton* **66**, 457-468.

Franklin, J. B. and Ullu, E. (2010). Biochemical analysis of PIFTC3, the Trypanosoma brucei orthologue of nematode DYF-13, reveals interactions with established and putative intraflagellar transport components. *Molecular microbiology* **78**, 173-186.

Goetz, S. C. and Anderson, K. V. (2010). The primary cilium: a signalling centre during vertebrate development. *Nature reviews. Genetics* **11**, 331-344.

Gurnett, C. A., Bowcock, A. M., Dietz, F. R., Morcuende, J. A., Murray, J. C. and Dobbs, M. B. (2007). Two novel point mutations in the long-range SHH enhancer in three families with triphalangeal thumb and preaxial polydactyly. *Am J Med Genet A* **143A**, 27-32.

Haycraft, C. J., Banizs, B., Aydin-Son, Y., Zhang, Q., Michaud, E. J. and Yoder, B. K. (2005). Gli2 and Gli3 localize to cilia and require the intraflagellar transport protein polaris for processing and function. *PLoS genetics* **1**, e53.

Hildebrandt, F., Benzing, T. and Katsanis, N. (2011). Ciliopathies. *The New England journal of medicine* **364**, 1533-1543.

Houde, C., Dickinson, R. J., Houtzager, V. M., Cullum, R., Montpetit, R., Metzler, M., Simpson, E. M., Roy, S., Hayden, M. R., Hoodless, P. A., et al. (2006). Hippi is

essential for node cilia assembly and Sonic hedgehog signaling. *Developmental biology* **300**, 523-533.

Hsiao, Y. C., Tuz, K. and Ferland, R. J. (2012). Trafficking in and to the primary cilium. *Cilia* **1**, 4.

Huangfu, D., Liu, A., Rakeman, A. S., Murcia, N. S., Niswander, L. and Anderson, K. V. (2003). Hedgehog signalling in the mouse requires intraflagellar transport proteins. *Nature* **426**, 83-87.

Ishikawa, H., Ide, T., Yagi, T., Jiang, X., Hirono, M., Sasaki, H., Yanagisawa, H., Wemmer, K. A., Stainier, D. Y., Qin, H., et al. (2014). TTC26/DYF13 is an intraflagellar transport protein required for transport of motility-related proteins into flagella. *eLife* **3**, e01566.

Johnson, D. R. and Hunt, D. M. (1971). Hop-sterile, a mutant gene affecting sperm tail development in the mouse. *Journal of embryology and experimental morphology* **25**, 223-236.

Katoh, Y., Terada, M., Nishijima, Y., Takei, R., Nozaki, S., Hamada, H. and Nakayama, K. (2016). Overall Architecture of the Intraflagellar Transport (IFT)-B Complex Containing Cluap1/IFT38 as an Essential Component of the IFT-B Peripheral Subcomplex. *The Journal of biological chemistry* **291**, 10962-10975.

Keady, B. T., Samtani, R., Tobita, K., Tsuchya, M., San Agustin, J. T., Follit, J. A., Jonassen, J. A., Subramanian, R., Lo, C. W. and Pazour, G. J. (2012a). IFT25 links the signal-dependent movement of Hedgehog components to intraflagellar transport. *Developmental cell* **22**, 940-951.

Keady, B. T., Samtani, R., Tobita, K., Tsuchya, M., San Agustin, J. T., Follit, J. A., Jonassen, J. A., Subramanian, R., Lo, C. W. and Pazour, G. J. (2012b). IFT25 Links the Signal-Dependent Movement of Hedgehog Components to Intraflagellar Transport. *Developmental cell* **22**, 940-951.

Kong, Y. (2011). Btrim: A fast, lightweight adapter and quality trimming program for next-generation sequencing technologies. *Genomics* **98**, 152-153.

Kozminski, K. G., Beech, P. L. and Rosenbaum, J. L. (1995). The Chlamydomonas kinesin-like protein FLA10 is involved in motility associated with the flagellar membrane. *The Journal of cell biology* **131**, 1517-1527.

Kozminski, K. G., Johnson, K. A., Forscher, P. and Rosenbaum, J. L. (1993). A motility in the eukaryotic flagellum unrelated to flagellar beating. *Proceedings of the National Academy of Sciences of the United States of America* **90**, 5519-5523.

Lancaster, M. A. and Gleeson, J. G. (2009). The primary cilium as a cellular signaling center: lessons from disease. *Current opinion in genetics & development* **19**, 220-229.

Lee, M. S., Hwang, K. S., Oh, H. W., Ji-Ae, K., Kim, H. T., Cho, H. S., Lee, J. J., Yeong Ko, J., Choi, J. H., Jeong, Y. M., et al. (2015). IFT46 plays an essential role in cilia development. *Developmental biology* **400**, 248-257.

Lettice, L. A. (2003). A long-range Shh enhancer regulates expression in the developing limb and fin and is associated with preaxial polydactyly. *Human molecular genetics* **12**, 1725-1735.

Li, H., Handsaker, B., Wysoker, A., Fennell, T., Ruan, J., Homer, N., Marth, G., Abecasis, G., Durbin, R. and Genome Project Data Processing, S. (2009). The Sequence Alignment/Map format and SAMtools. *Bioinformatics* **25**, 2078-2079.

Liem, K. F., Jr., Ashe, A., He, M., Satir, P., Moran, J., Beier, D., Wicking, C. and Anderson, K. V. (2012). The IFT-A complex regulates Shh signaling through cilia structure and membrane protein trafficking. *The Journal of cell biology* **197**, 789-800.

Liew, G. M., Ye, F., Nager, A. R., Murphy, J. P., Lee, J. S., Aguiar, M., Breslow, D. K., Gygi, S. P. and Nachury, M. V. (2014). The Intraflagellar Transport Protein IFT27 Promotes BBSome Exit from Cilia through the GTPase ARL6/BBS3. *Developmental cell* **31**, 265-278.

Litingtung, Y. and Chiang, C. (2000). Specification of ventral neuron types is mediated by an antagonistic interaction between Shh and Gli3. *Nature neuroscience* **3**, 979-985.

Litingtung, Y., Dahn, R. D., Li, Y., Fallon, J. F. and Chiang, C. (2002). Shh and Gli3 are dispensable for limb skeleton formation but regulate digit number and identity. *Nature* **418**, 979-983.

Liu, A., Wang, B. and Niswander, L. A. (2005). Mouse intraflagellar transport proteins regulate both the activator and repressor functions of Gli transcription factors. *Development (Cambridge, England)* **132**, 3103-3111.

Marszalek, J. R., Ruiz-Lozano, P., Roberts, E., Chien, K. R. and Goldstein, L. S. B. (1999). Situs inversus and embryonic ciliary morphogenesis defects in mouse mutants lacking the KIF3A subunit of kinesin-II. *Proceedings of the National Academy of Sciences of the United States of America* **96**, 5043-5048.

Marti, E., Bumcrot, D. A., Takada, R. and McMahon, A. P. (1995). Requirement of 19K form of Sonic hedgehog for induction of distinct ventral cell types in CNS explants. *Nature* **375**, 322-325.

May, S. R., Ashique, A. M., Karlen, M., Wang, B., Shen, Y., Zarbalis, K., Reiter, J., Ericson, J. and Peterson, A. S. (2005). Loss of the retrograde motor for IFT disrupts localization of Smo to cilia and prevents the expression of both activator and repressor functions of Gli. *Developmental biology* **287**, 378-389.

Mill, P., Lockhart, Paul J., Fitzpatrick, E., Mountford, Hayley S., Hall, Emma A., Reijns, Martin A. M., Keighren, M., Bahlo, M., Bromhead, Catherine J., Budd, P., et al. (2011). Human and Mouse Mutations in WDR35 Cause Short-Rib Polydactyly Syndromes Due to Abnormal Ciliogenesis. *The American Journal of Human Genetics* **88**, 508-515.

Nagy, A., Gertsenstain, M., Vintersten, K. and Behringer, R. R. (2002). *Manipulating the Mouse Embryo: A Laboratory Manual* (3rd edn). Cold Spring Harbor, NY: Cold Spring Harbor Laboratory Press.

Nagy, A. G., M., Vintersten, K., Behringer, R. (2003). *Manipulating the Mouse Embryo: A Laboratory Manual*. Cold Spring Harbor, NY: Cold Spring Harbor Laboratory Press.

Nigg, E. A. and Raff, J. W. (2009). Centrioles, centrosomes, and cilia in health and disease. *Cell* **139**, 663-678.

Oh, E. C. and Katsanis, N. (2012). Cilia in vertebrate development and disease. *Development (Cambridge, England)* **139**, 443-448.

Ou, Y., Ruan, Y., Cheng, M., Moser, J. J., Rattner, J. B. and van der Hoorn, F. A. (2009). Adenylate cyclase regulates elongation of mammalian primary cilia. *Experimental cell research* **315**, 2802-2817.

Park, K., Kang, J., Subedi, K. P., Ha, J. H. and Park, C. (2008). Canine polydactyl mutations with heterogeneous origin in the conserved intronic sequence of LMBR1. *Genetics* **179**, 2163-2172.

Pazour, G. J., Wilkerson, C. G. and Witman, G. B. (1998). A dynein light chain is essential for the retrograde particle movement of intraflagellar transport (IFT). *The Journal of cell biology* **141**, 979-992.

Pedersen, L. B., Veland, I. R., Schroder, J. M. and Christensen, S. T. (2008). Assembly of primary cilia. *Dev Dyn* **237**, 1993-2006.

Pruitt, K. D., Harrow, J., Harte, R. A., Wallin, C., Diekhans, M., Maglott, D. R., Searle, S., Farrell, C. M., Loveland, J. E., Ruef, B. J., et al. (2009). The consensus coding sequence (CCDS) project: Identifying a common protein-coding gene set for the human and mouse genomes (vol 19, pg 1316, 2009). *Genome Res* **19**, 1506-1506.

Qin, J., Lin, Y., Norman, R. X., Ko, H. W. and Eggenschwiler, J. T. (2011). Intraflagellar transport protein 122 antagonizes Sonic Hedgehog signaling and controls ciliary localization of pathway components. *Proceedings of the National Academy of Sciences of the United States of America* **108**, 1456-1461.

Rohatgi, R., Milenkovic, L. and Scott, M. P. (2007). Patched1 regulates hedgehog signaling at the primary cilium. *Science* **317**, 372-376.

Rosenbaum, J. L. and Witman, G. B. (2002). Intraflagellar transport. *Nat Rev Mol Cell Bio* **3**, 813-825.

Sharma, N., Berbari, N. F. and Yoder, B. K. (2008a). Chapter 13 Ciliary Dysfunction in Developmental Abnormalities and Diseases. **85**, 371-427.

Sharma, N., Berbari, N. F. and Yoder, B. K. (2008b). Ciliary dysfunction in developmental abnormalities and diseases. *Current topics in developmental biology* **85**, 371-427.

Sharpe, J., Lettice, L., Hecksher-Sorensen, J., Fox, M., Hill, R. and Krumlauf, R. (1999). Identification of sonic hedgehog as a candidate gene responsible for the polydactylous mouse mutant Sasquatch. *Current biology : CB* **9**, 97-100.

Sun, M., Ma, F., Zeng, X., Liu, Q., Zhao, X. L., Wu, F. X., Wu, G. P., Zhang, Z. F., Gu, B., Zhao, Y. F., et al. (2008). Triphalangeal thumb-polysyndactyly syndrome and syndactyly type IV are caused by genomic duplications involving the long range, limb-specific SHH enhancer. *J Med Genet* **45**, 589-595.

Swiderski, R. E., Nakano, Y., Mullins, R. F., Seo, S. and Banfi, B. (2014). A mutation in the mouse ttc26 gene leads to impaired hedgehog signaling. *PLoS genetics* **10**, e1004689.

Taschner, M., Kotsis, F., Braeuer, P., Kuehn, E. W. and Lorentzen, E. (2014). Crystal structures of IFT70/52 and IFT52/46 provide insight into intraflagellar transport B core complex assembly. *The Journal of cell biology* **207**, 269-282.

Taschner, M., Weber, K., Mourao, A., Vetter, M., Awasthi, M., Stiegler, M., Bhogaraju, S. and Lorentzen, E. (2016). Intraflagellar transport proteins 172, 80, 57, 54, 38, and 20 form a stable tubulin-binding IFT-B2 complex. *The EMBO journal*.

te Welscher, P., Zuniga, A., Kuijper, S., Drenth, T., Goedemans, H. J., Meijlink, F. and Zeller, R. (2002). Progression of vertebrate limb development through SHH-mediated counteraction of GLI3. *Science* **298**, 827-830.

Tran, P. V., Haycraft, C. J., Besschetnova, T. Y., Turbe-Doan, A., Stottmann, R. W., Herron, B. J., Chesebro, A. L., Qiu, H., Scherz, P. J., Shah, J. V., et al. (2008). THM1 negatively modulates mouse sonic hedgehog signal transduction and affects retrograde intraflagellar transport in cilia. *Nature genetics* **40**, 403-410.

Vokes, S. A., Ji, H. K., Wong, W. H. and McMahon, A. P. (2008). A genome-scale analysis of the cis-regulatory circuitry underlying sonic hedgehog-mediated patterning of the mammalian limb. *Genes & development* **22**, 2651-2663.

Wang, C., Ruther, U. and Wang, B. (2007). The Shh-independent activator function of the full-length Gli3 protein and its role in vertebrate limb digit patterning. *Developmental biology* **305**, 460-469.

Wang, Z., Phan, T. and Storm, D. R. (2011). The type 3 adenylyl cyclase is required for novel object learning and extinction of contextual memory: role of cAMP signaling in primary cilia. *The Journal of neuroscience : the official journal of the Society for Neuroscience* **31**, 5557-5561.

Waters, A. M. and Beales, P. L. (2011). Ciliopathies: an expanding disease spectrum. *Pediatric nephrology (Berlin, Germany)* **26**, 1039-1056.

Weatherbee, S. D., Niswander, L. A. and Anderson, K. V. (2009). A mouse model for Meckel syndrome reveals Mks1 is required for ciliogenesis and Hedgehog signaling. *Human molecular genetics* **18**, 4565-4575.

Zhang, Q., Liu, Q., Austin, C., Drummond, I. and Pierce, E. A. (2012). Knockdown of ttc26 disrupts ciliogenesis of the photoreceptor cells and the pronephros in zebrafish. *Molecular biology of the cell* **23**, 3069-3078.

Figures

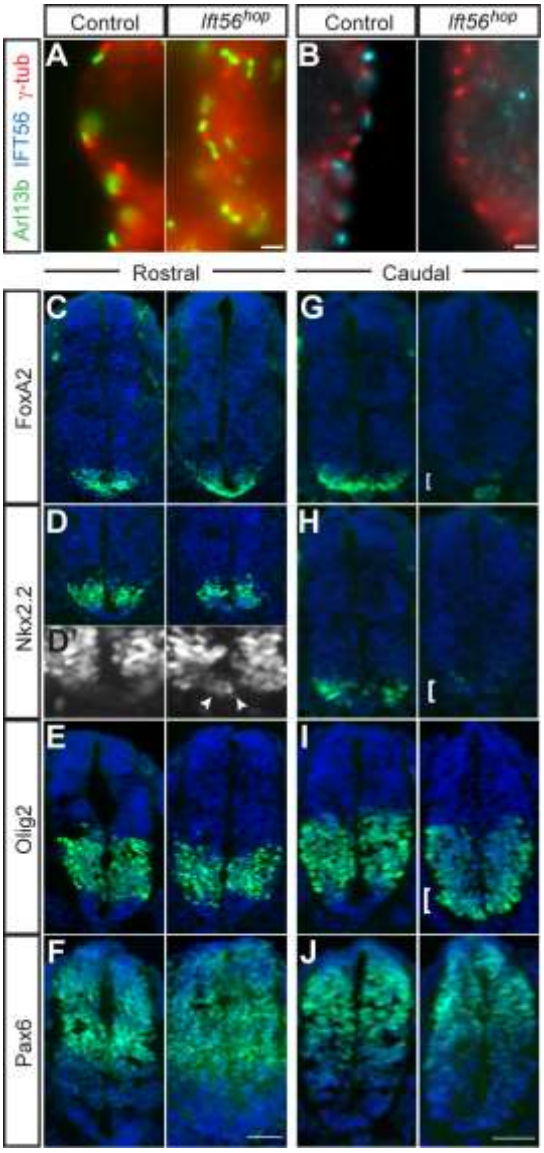

Figure 1. *Ift56*^{hop} neural tube cilia show reduced sensitivity to Shh signaling. (**A,B**) *Ift56*^{hop} neural tubes form a similar number of cilia as controls, but lack IFT56 protein. Neural tube sections were stained for Arl13b (green) to mark ciliary axonemes, or IFT56 (cyan), and γ-tubulin to mark basal bodies (red). (**C-J**) e10.5 neural tube sections were stained with DAPI (blue) and markers of neuronal progenitors (green). (**C,G**) FoxA2 is expressed normally in the rostral (forelimb region) floor plate in *Ift56*^{hop} neural tubes and dramatically reduced caudally (hindlimb region). A subset of V3 interneuron progenitors (Nkx2.2) are

misplaced and found at the *Ift56*^{hop} midline rostrally (**D,D'**, arrowheads in inset) and almost completely absent caudally (**H**; bracket). Motorneuron progenitors (Olig2) are unaffected in rostral *Ift56*^{hop} sections (**E**) but are specified throughout the entire ventral caudal neural tube (**I**; bracket). Pax6 appears unaffected throughout the *Ift56*^{hop} neural tube (**F,J**). n=3 biological replicates each from control and mutant, 3 sections per replicate were analyzed. Scale bars=2uM (**A,B**), 100uM (**C-J**).

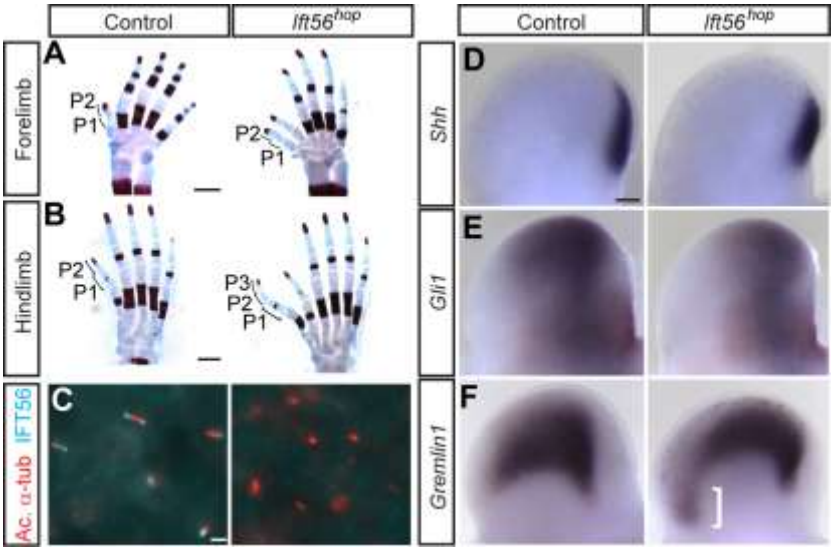

Figure 2. *Ift56*^{hop} mutants develop preaxial polydactyly due to impaired Gli3R function. e18.5 *Ift56*^{hop} forelimbs (**A**) develop a duplication of the anterior digit (2 phalanges; P1, P2) and hindlimbs either form an extra anterior digit (not shown) or a digit with more posterior morphology (**B**; 3 phalanges: P1, P2, P3) preaxially. Alizarin red marks bone and Alcian blue marks cartilage. n=5 biological replicates each from control and mutant for skeletal analyses. (**C**) *Ift56*^{hop} limb mesenchyme form cilia but lack IFT56 protein. Cilia were stained for acetylated α-tubulin (red) to mark ciliary axonemes and IFT56 (cyan). (**D**) At e11.5, *Ift56*^{hop} limb buds express Shh in a posterior domain similar to controls. (**E**) *Gli1*, a direct positive target of Shh, is expressed in a relatively normal posterior domain in *Ift56*^{hop}. In contrast, *Gremlin1,* which is normally inhibited by Gli3R in anterior limbs, shows an ectopic anterior domain of expression in *Ift56*^{hop} mutant limb buds (**F**; bracket). n=3 biological replicates each from control and mutant, 3 sections per replicate were analyzed. Scale bars=0.5mm (**A**), 1mm (**B**), 2uM (**C**), 0.1mm (**D-F**).

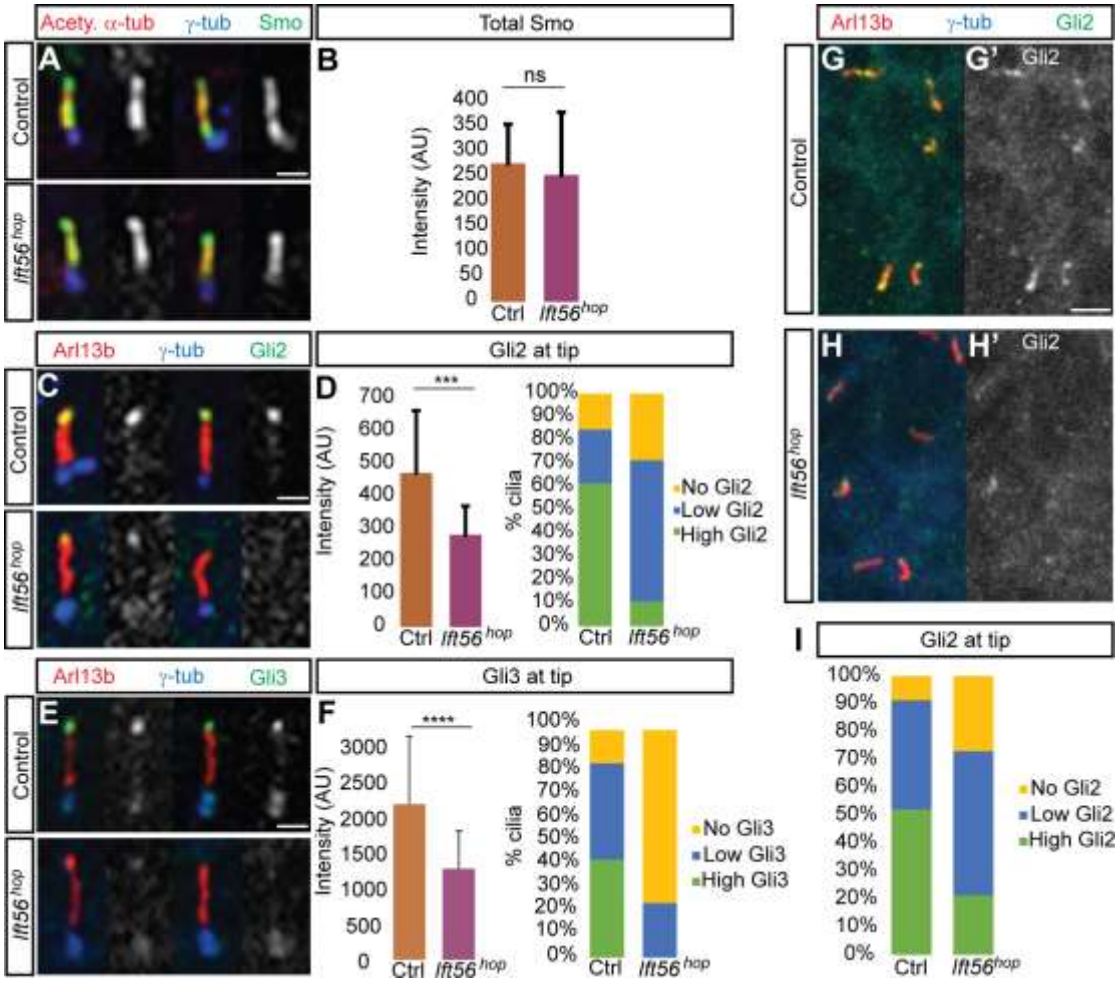

Figure 3. Ciliary localization of Gli proteins is disrupted in *Ift56*^{hop} cells. (**A,B**) Ciliary levels of Smo are unchanged in *Ift56*^{hop} MEF cilia in response to activation of the Shh pathway via SAG treatment (control n=12, mutant n=10 cilia counted in representative MEF line). (**C,D**) In *Ift56*^{hop} cilia, mean Gli2 tip accumulation is significantly decreased and over half of the mutant cilia completely lack Gli2 (control n=17, mutant n=20 cilia counted in representative MEF line). (**E,F**) Similar to Gli2, mean Gli3 accumulation is significantly decreased in *Ift56*^{hop}cilia and ~80% of mutant cilia lacked Gli3 at the distal tip (control n=36, mutant n=21 cilia counted in representative MEF line). (**G,H**) Limb mesenchyme cilia were assayed for with Gli2 (green) and Arl13b (red) to mark ciliary axonemes. Representative images were taken in the posterior limb bud of caudal (hindlimb) regions. (**G',H')** Gli2-only channel is shown in Black and White. (**I**) *Ift56*^{hop} mutants displayed fewer cilia with high levels of Gli2 and more cilia with low and absent Gli2 (control n=92, mutant n=89 cilia counted). (**D,F** *** denotes p<0.001, **** denotes p<0.0001 by two-tailed student's t-test with

unequal variances, all data are calculated as mean±s.d.). n=4 biological replicates each from control and mutant for MEFs and tissue, and 3 sections per replicate were analyzed in tissue. Scale bars=3uM (**A,C,E**), 2uM (**G,H**).

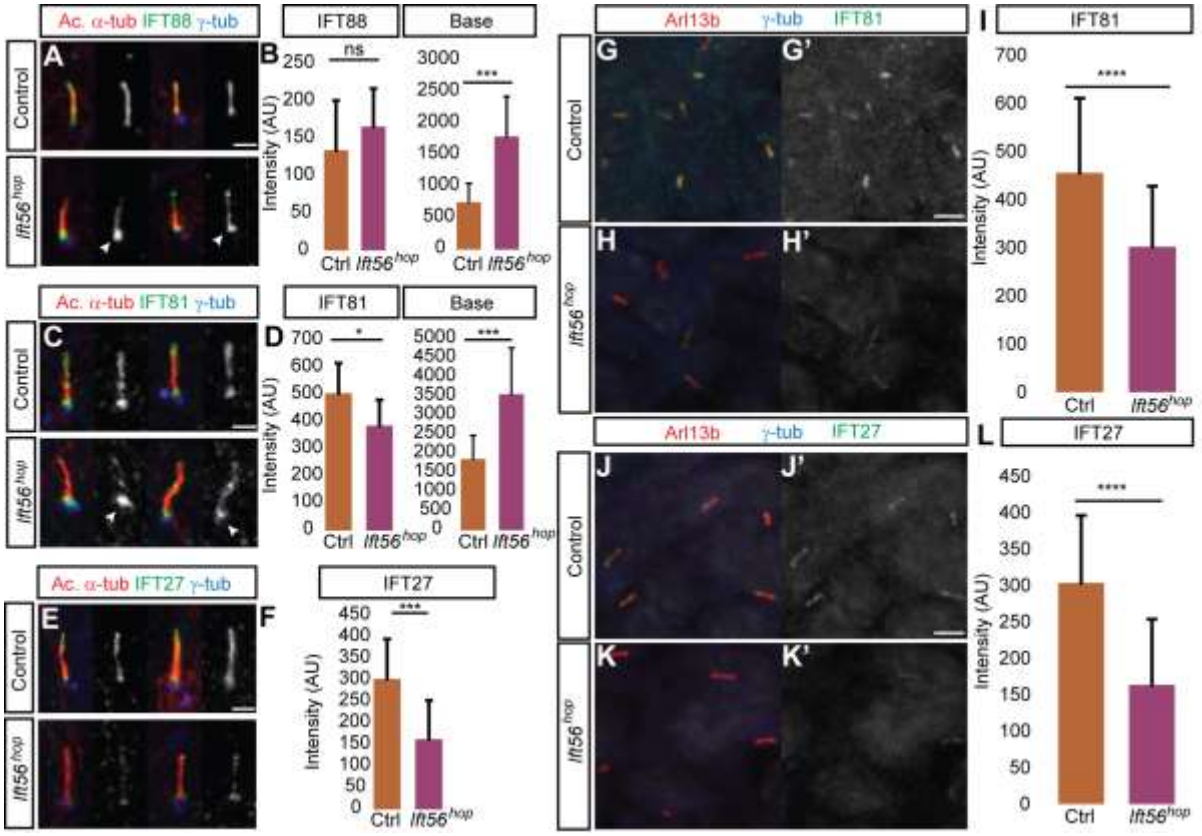

Figure 4. The integrity of the IFTB complex breaks down in *Ift56*^{hop} cilia. (**A,B**) While axonemal levels of IFT88 were comparable to controls, a pool of IFT88 accumulated at the base of *Ift56*^{hop} MEF cilia (control n=9, mutant n=13 cilia counted in representative MEF line). (**C,D**) Axonemal levels of IFT81 were significantly decreased and a pool of IFT81 was found at the base of *Ift56*^{hop} cilia (control n=15, mutant n=15 cilia counted in representative MEF line). (**E,F**) IFT27 did not pool at the base of *Ift56*^{hop} cilia but showed ~50% reduction in ciliary axonemes (control n=21, mutant n=22 cilia counted in representative MEF line). (**G-K**) *in vivo* analyses supported the MEF results, showing a significant reduction of IFT81 and IFT27 in *Ift56*^{hop} limb mesenchyme cilia (n=4 biological replicates each from control and mutant, and 3 sections per replicate were analyzed). (**G'-H')** The IFT-only channel is shown in Black and White. (**I,L**) Both IFT81 and IFT27 within *Ift56*^{hop} mutant limb cilia are significantly decreased compared to control cilia (n=35 cilia from each control and mutant counted for each IFT). **A,C,E;** MEFs were immunostained for specific IFT proteins (green), acetylated α-tubulin to mark axonemes (red), and γ-tubulin to mark basal bodies (blue). **G-K;** Limb mesenchyme cilia were immunostained for specific IFT proteins (green), Arl13b to

mark axonemes (red). (**** denotes p<0.0001, *** denotes p<0.001, * denotes p<0.05 by two-tailed student's t-test with unequal (**A-E**)/equal (**G-K**) variances, all data are calculated as mean±s.d.). Scale bars=3uM (**A-E**), 2uM (**G-K**).

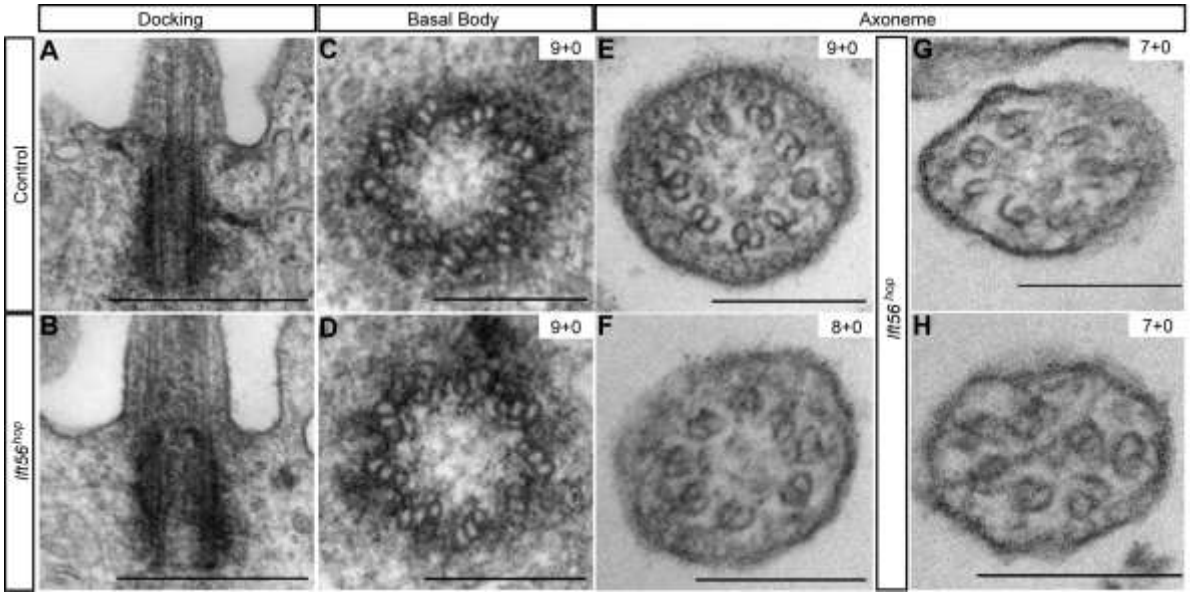

Figure 5. Ciliary axonemal microtubule organization and number is altered in *Ift56*^{hop} mutants. (**A,B**) Transmission electron microscopy on e11.5 neural tube cilia revealed normal basal body docking and ciliary outgrowth in *Ift56*^{hop} mutants. (**C,D**) Cross sections through the basal body showed a normal structure of 9+0 triplet microtubules in mutants. (**F-H**) Axonemal cross sections revealed reduced numbers of microtubule doublets in *Ift56*^{hop} cilia (e.g. 8+0 and 7+0) and a disruption of the normal circular arrangement of doublets (**E**). All imaging and analysis were performed in the posterior neural tube along the ventral wall (n=2 sections analyzed for each sample, with 3 biological replicates of each control and mutant). Scale bars=500nM.

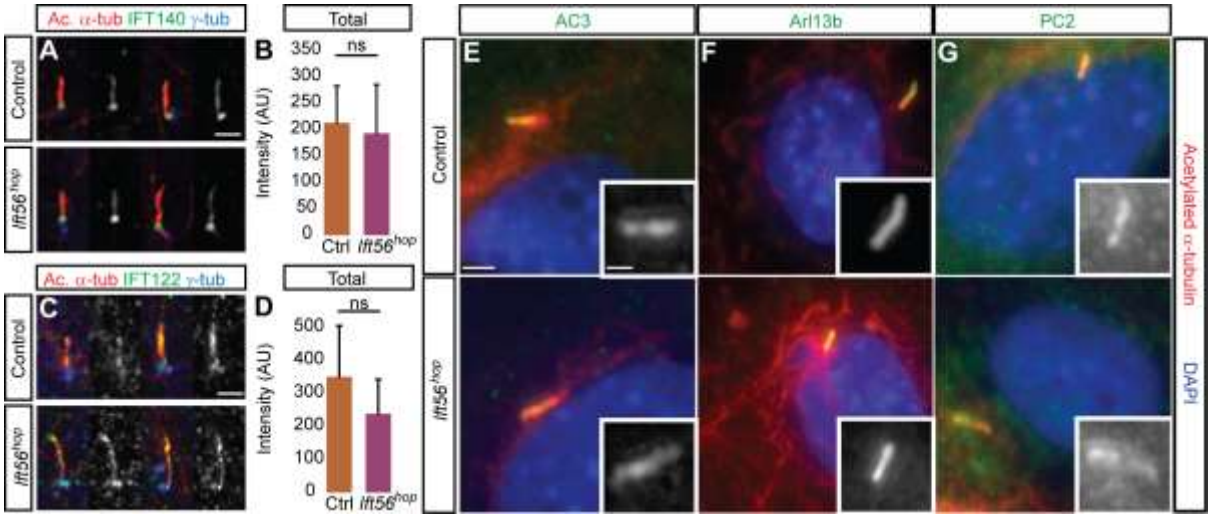

Figure 6. IFTA components and IFTA-dependent proteins localize normally in *Ift56*^{hop} cilia. (**A,B**) IFT140 (control n=14, mutant n=16 cilia counted in representative MEF line) and (**C,D**) IFT122 (control n=9, mutant n=13 cilia counted in representative MEF line) proteins localize normally and are found at similar levels in *Ift56*^{hop} and control cilia. (**E-G**) AC3, Arl13b, and PC2 are critical for cilia function and do not require IFT56 for their localization. **A,C**; MEFs were immunostained for specific IFT proteins (green), acetylated α-tubulin to mark axonemes (red), and γ-tubulin to mark basal bodies (n=4 biological replicates each from control and mutant, and 2 technical replicates were analyzed). (**E-G**) MEFs were immunostained with acetylated α-tubulin (red), specific ciliary proteins (green), and DAPI (blue). Inset shows higher magnification of ciliary protein expression in black and white. Scale bars=3uM (**A,C**), 2uM (**E-G**), 1uM (**E-G inset**).

SUPPLEMENTAL MATERIALS AND METHODS

Primary Antibodies

Pax6 was deposited to the DSHB by Kawakami, A. (DSHB Hybridoma Product PAX6). Nkx6.1 was deposited to the DSHB by Madsen, O.D. (DSHB Hybridoma Product F64A6B4). Nkx2.2 was deposited to the DSHB by Jessell, T.M. / Brenner-Morton, S. (DSHB Hybridoma Product 74.5A5) Pax6, Nkx6.1, and Nkx2.2 were used at 1:100. Anti-Olig2 was obtained from Millipore (catalog number MABN50) and used at 1:200. Anti-Acetylated α-tubulin was obtained from Sigma-Aldrich (catalog number T7451,) and used at 1:2000. Anti-γ-tubulin was obtained from Sigma-Aldrich (catalog number T5326) and used at 1:2000. Anti-IFT56 was obtained from Novus Biologicals (catalog number NBP1-84034) and used at 1:500. Anti-FoxA2 was obtained from Abcam (catalog number), Anti-ACIII was obtained from Santa Cruz (catalog number sc-588) and used at 1:200. Anti-Flag was obtained from Sigma-Aldrich (catalog number F7425) and used at 1:2000. Anti-PC2 (gift from Stefan Somlo) was used at 1:500, Anti-Arl13b (gift from Tamara Caspary) was used at 1:2000, Anti-Gli2 (gift from Jonathan Eggenschwiler) was used at 1:1000, Anti-Gli3 (gift from Suzie Scales) was used at 1:1000. Anti-IFT81 was obtained from Proteintech (catalog number 11744-1-AP) and used at 1:1000. Anti-IFT88 was obtained from Proteintech (catalog number 13967-1-AP) and used at 1:500. Anti-IFT27 (gift from Greg Pazour) was used at 1:1000, anti-IFT140 (gift from Greg Pazour) was used at 1:1000, and anti-IFT122 (gift from Jonathan Eggenschwiler) was used at 1:500.

Real-Time-PCR and analysis

Total RNA was extracted from e11 limb buds using standard protocol with TRIzol (Invitrogen). cDNA was reverse transcribed using the SuperScript III kit (Invitrogen). qRT-PCR was performed using *Power* SYBR Green PCR Master Mix (Applied Biosystems) on a ViiA7 Real-Time PCR system (Applied Biosystems). Relative transcript expression levels were determined by the standard comparative C_T method (Schmittgen and Livak, 2008).

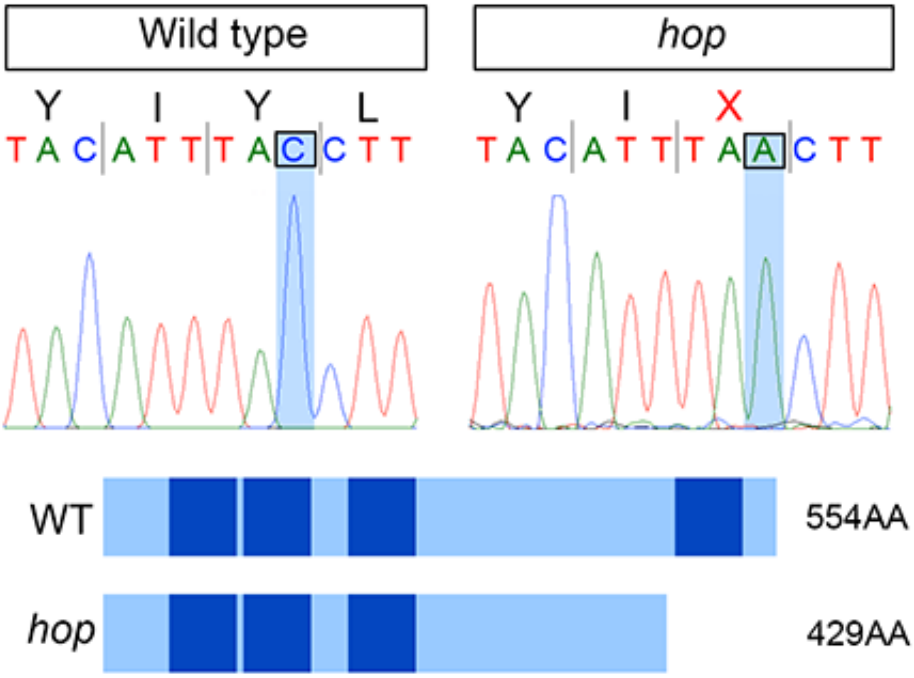

Figure S1. Sanger sequencing traces revealed that the *Ift56*^{hop} mutation is a cytosine-to-adenosine transversion (c.1290**C>A**) at mouse Chr6:38,362,071 within the coding region of *Ift56*, resulting in a truncation of the C-terminus (**Y430X**) and loss of the 4th TPR domain (dark blue shading) of the IFT56 protein product.

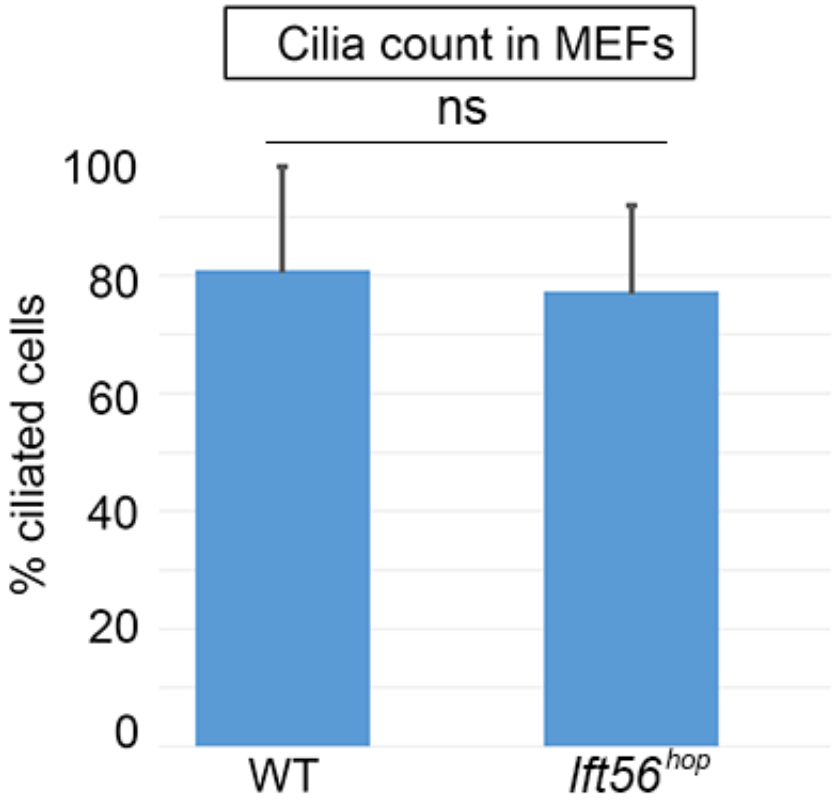

Figure S2. The percentage of ciliated MEFs was not significantly different between control and *Ift56*^{hop} cells. Cilia were marked by acetylated α-tubulin, and at least 3 slides were imaged for 3 or more control and mutants. At least 50 total cells were counted for ciliation per sample.

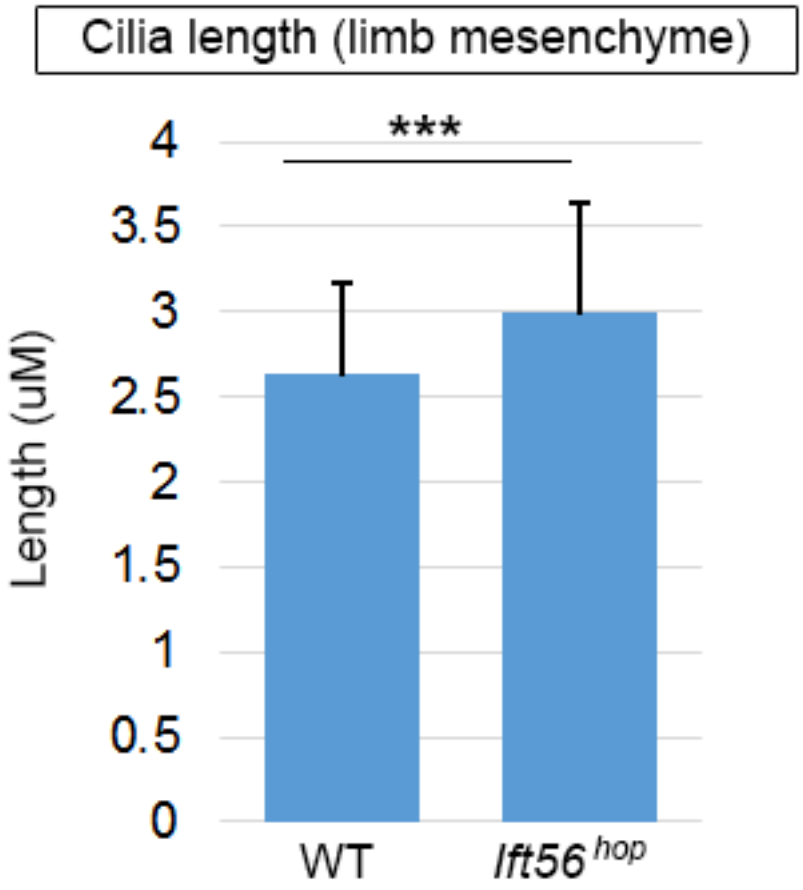

Figure S3. Cilia in the limb mesenchyme of *Ift56*^{hop} mutants are significantly longer compared to control animals. Cilia were marked by Arl13b, and at least 3 slides were imaged for 3 or more control and mutants. At least 30 total cells were counted for ciliation per sample.

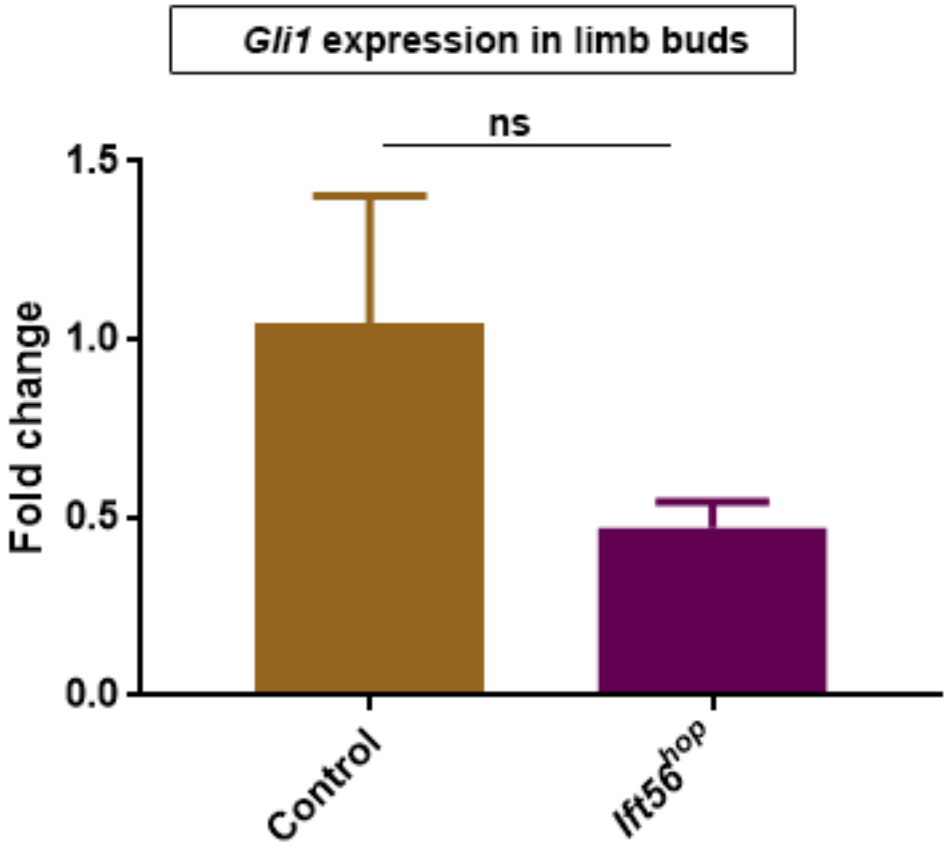

Figure S4. *Gli1* transcript levels in the *Ift56*^{hop} limb buds are reduced but not quite significant (p=0.0531 by unpaired two-tailed student's t-test with equal variances, data is calculated as mean±s.d). 3 technical replicates were performed per sample for 3 controls and 3 mutants.

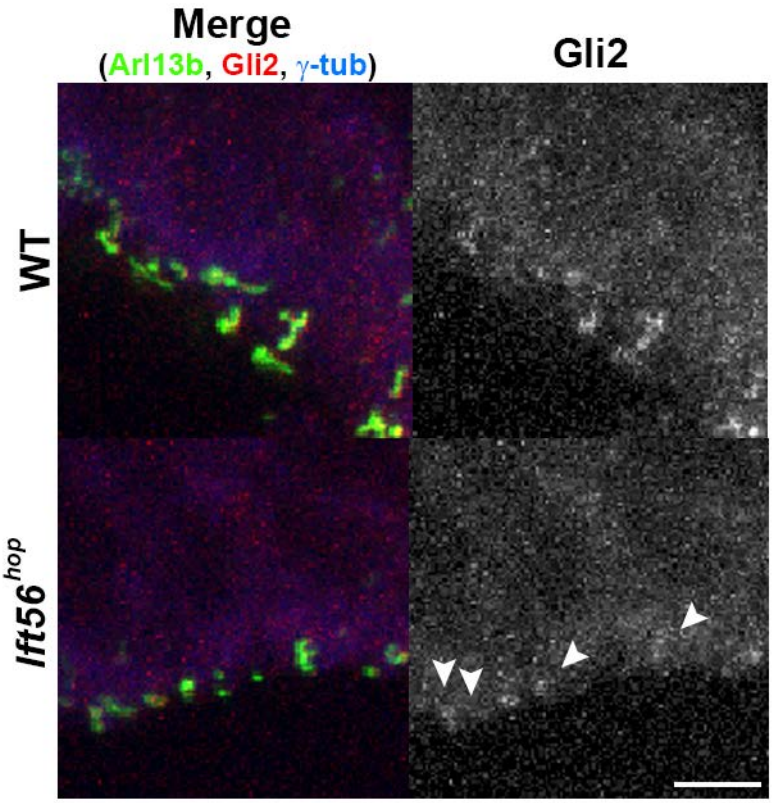

Figure S5. Neural tube cilia were assayed for with Gli2 (red) and Arl13b (green) to mark ciliary axonemes. Gli2-only channel (right) shows fainter Gli2 in *Ift56*^{hop} cilia (arrowheads). Representative images were taken along the ventral wall of caudal (hindlimb) regions. At least 3 sections were imaged per sample of 4 or more controls and mutants.

SUPPLEMENTAL MATERIALS AND METHODS

Primary Antibodies

Pax6 was deposited to the DSHB by Kawakami, A. (DSHB Hybridoma Product PAX6). Nkx6.1 was deposited to the DSHB by Madsen, O.D. (DSHB Hybridoma Product F64A6B4). Nkx2.2 was deposited to the DSHB by Jessell, T.M. / Brenner-Morton, S. (DSHB Hybridoma Product 74.5A5) Pax6, Nkx6.1, and Nkx2.2 were used at 1:100. Anti-Olig2 was obtained from Millipore (catalog number MABN50) and used at 1:200. Anti-Acetylated α-tubulin was obtained from Sigma-Aldrich (catalog number T7451,) and used at 1:2000. Anti-γ-tubulin was obtained from Sigma-Aldrich (catalog number T5326) and used at 1:2000. Anti-IFT56 was obtained from Novus Biologicals (catalog number NBP1-84034) and used at 1:500. Anti-FoxA2 was obtained from Abcam (catalog number), Anti-ACIII was obtained from Santa Cruz (catalog number sc-588) and used at 1:200. Anti-Flag was obtained from Sigma-Aldrich (catalog number F7425) and used at 1:2000. Anti-PC2 (gift from Stefan Somlo) was used at 1:500, Anti-Arl13b (gift from Tamara Caspary) was used at 1:2000, Anti-Gli2 (gift from Jonathan Eggenschwiler) was used at 1:1000, Anti-Gli3 (gift from Suzie Scales) was used at 1:1000. Anti-IFT81 was obtained from Proteintech (catalog number 11744-1-AP) and used at 1:1000. Anti-IFT88 was obtained from Proteintech (catalog number 13967-1-AP) and used at 1:500. Anti-IFT27 (gift from Greg Pazour) was used at 1:1000, anti-IFT140 (gift from Greg Pazour) was used at 1:1000, and anti-IFT122 (gift from Jonathan Eggenschwiler) was used at 1:500.

Secondary Antibodies

Alexa Fluor 633 goat anti-mouse IgG was obtained from Molecular Probes Inc. (catalog number A21052) and used at 1:500. Alexa Fluor 533 goat anti-mouse IgG1 was obtained from Molecular Probes Inc. (catalog number A21126) and used at 1:500. Cy3-conjugated AffiniPure goat anti-mouse IgG was obtained from Jackson ImmunoResearch Laboratories

Inc. (catalog number 115-165-166) and used at 1:500. Alexa Fluor 568 goat anti-mouse IgG2b was obtained from Molecular Probes Inc. (catalog number A21144) and used at 1:500. Cy3-conjugated AffiniPure goat anti-mouse IgG2a was obtained from Jackson ImmunoResearch Laboratories Inc. (catalog number 115-165-206) and used at 1:500. Cy3-conjugated AffiniPure goat antimouse IgG2b was obtained from Jackson ImmunoResearch Laboratories Inc. (catalog number 115-165-207) and used at 1:500. Alexa Fluor 488 goat anti-mouse IgG1 was obtained from Jackson ImmunoResearch Laboratories Inc. (catalog number 115-545-205) and used at 1:500.

Riboprobes

The *Gli1* riboprobe plasmid (pBluescript) was a gift from Josh Catron. The *Shh* riboprobe plasmid (pBluescript II) was a gift from Andrew McMahon. The *Gremlin1* riboprobe plasmid (pBluescript) was a gift from Richard Harland.

Real-Time-PCR and analysis

Total RNA was extracted from e11 limb buds using standard protocol with TRIzol (Invitrogen). cDNA was reverse transcribed using the SuperScript III kit (Invitrogen). qRT-PCR was performed using *Power* SYBR Green PCR Master Mix (Applied Biosystems) on a ViiA7 Real-Time PCR system (Applied Biosystems). Relative transcript expression levels were determined by the standard comparative C_T method (Schmittgen and Livak, 2008).

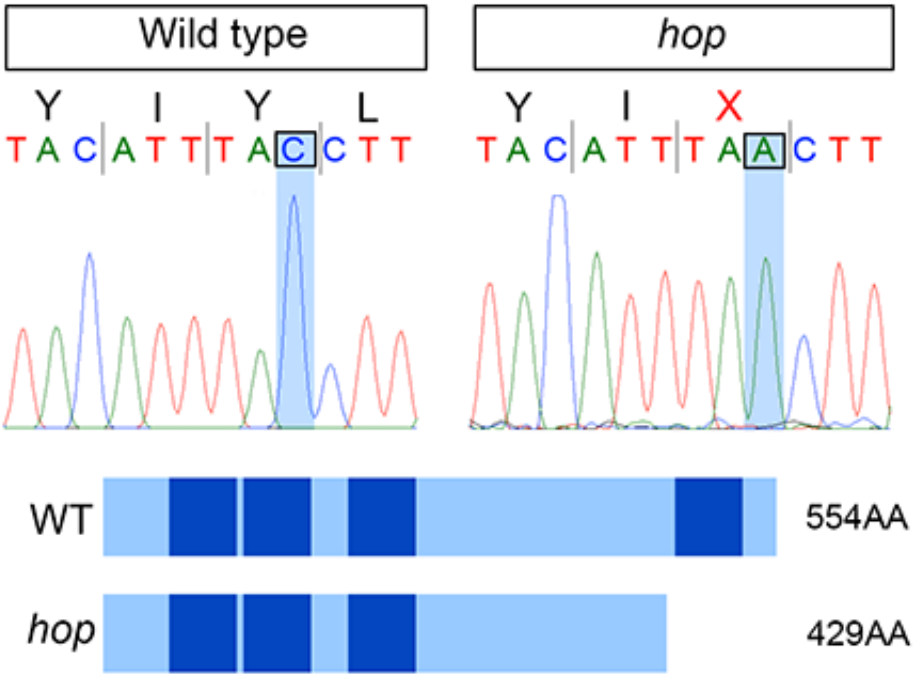

Figure S1. Sanger sequencing traces revealed that the *Ift56*^{hop} mutation is a cytosine-to-adenosine transversion (c.1290**C>A**) at mouse Chr6:38,362,071 within the coding region of *Ift56*, resulting in a truncation of the C-terminus (**Y430X**) and loss of the 4th TPR domain (dark blue shading) of the IFT56 protein product.

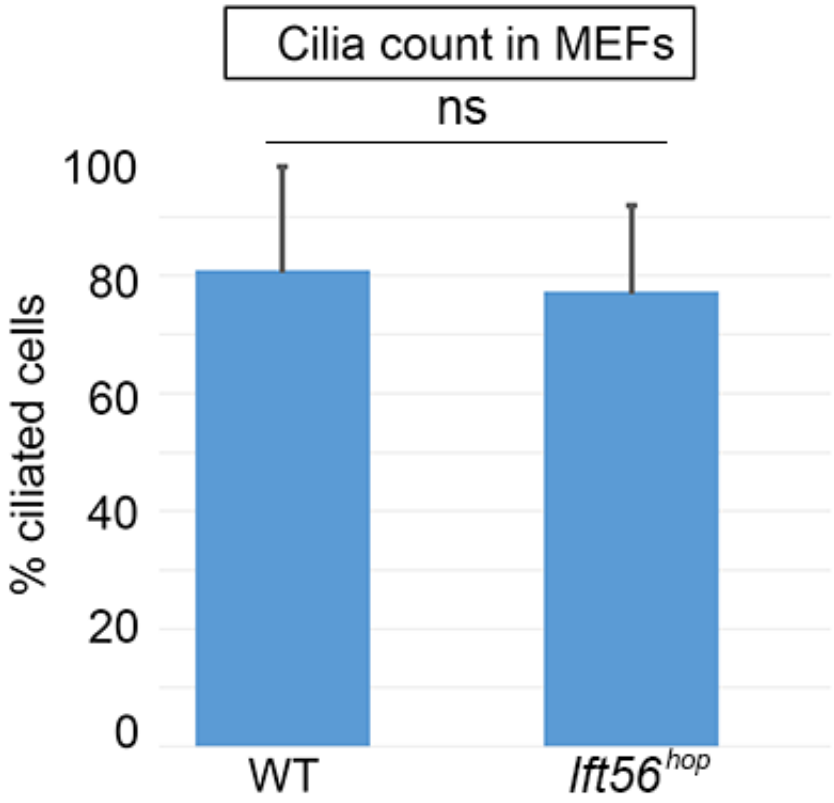

Figure S2. The percentage of ciliated MEFs was not significantly different between control and *Ift56*^{hop} cells. Cilia were marked by acetylated α-tubulin, and at least 3 slides were imaged for 3 or more control and mutants. At least 50 total cells were counted for ciliation per sample.

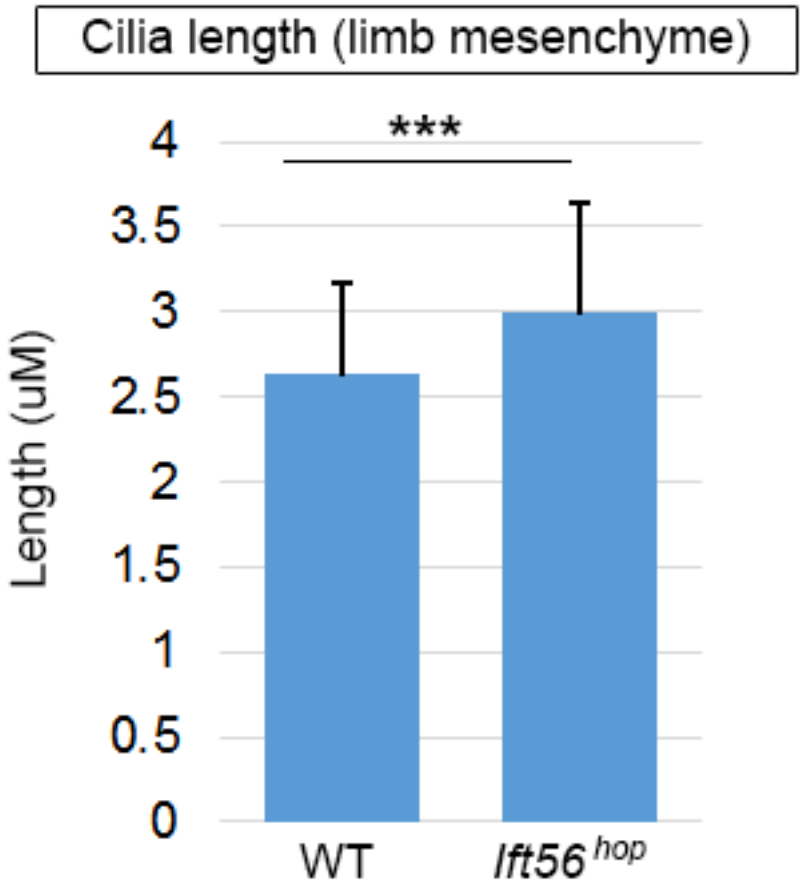

Figure S3. Cilia in the limb mesenchyme of *Ift56*^{hop} mutants are significantly longer compared to control animals. Cilia were marked by Arl13b, and at least 3 slides were imaged for 3 or more control and mutants. At least 30 total cells were counted for ciliation per sample.

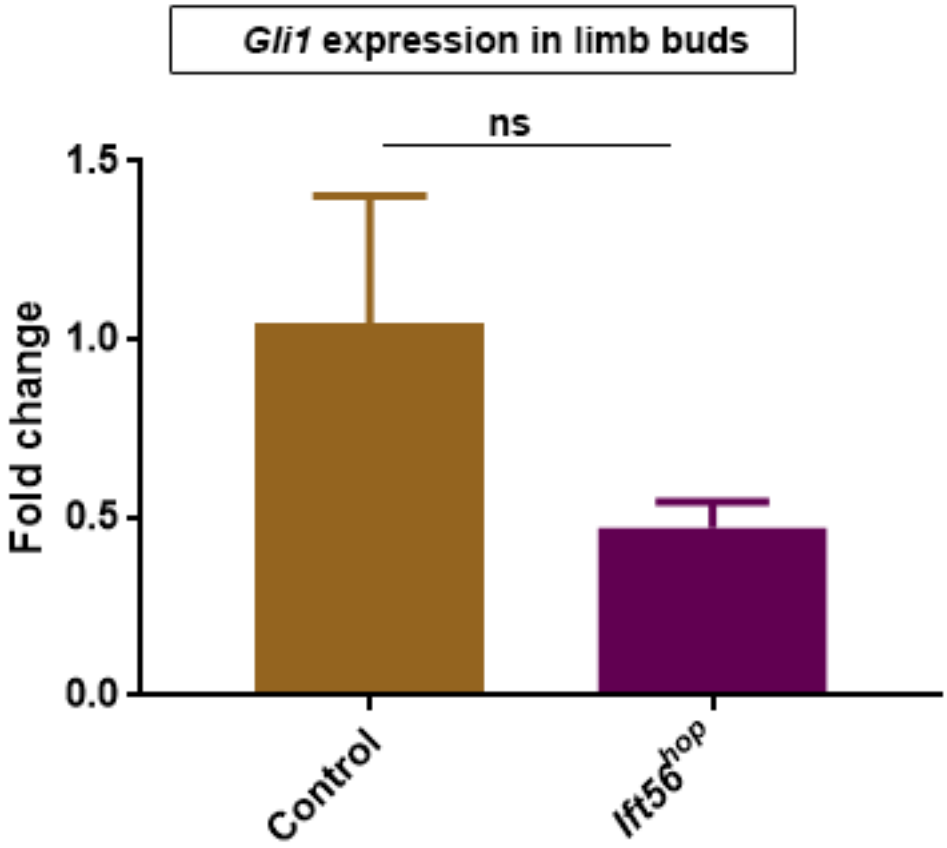

Figure S4. *Gli1* transcript levels in the *Ift56*^{hop} limb buds are reduced but not quite significant (p=0.0531 by unpaired two-tailed student's t-test with equal variances, data is calculated as mean±s.d). 3 technical replicates were performed per sample for 3 controls and 3 mutants.

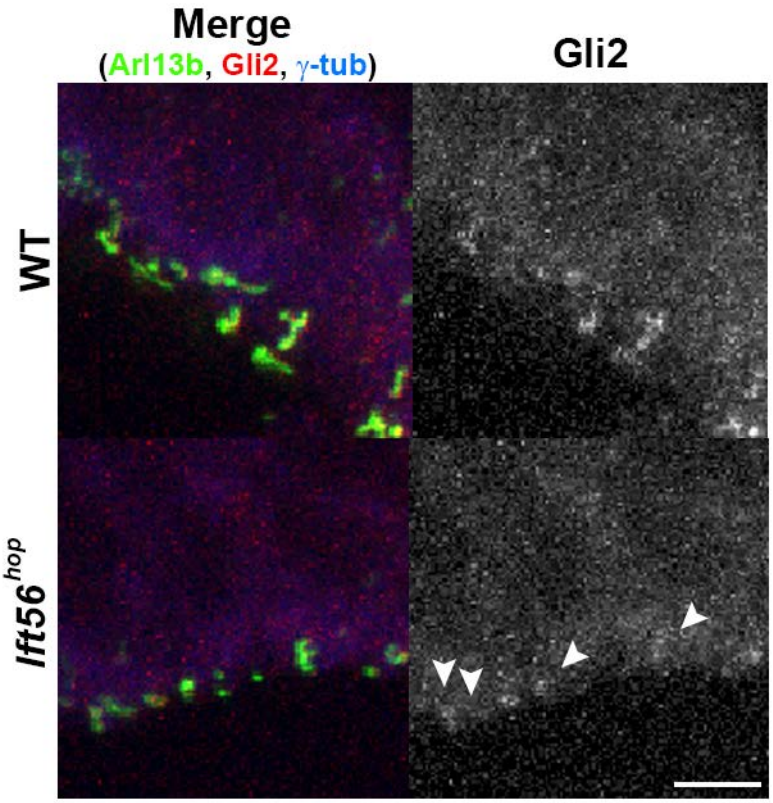

Figure S5. Neural tube cilia were assayed for with Gli2 (red) and Arl13b (green) to mark ciliary axonemes. Gli2-only channel (right) shows fainter Gli2 in *Ift56*^{hop} cilia (arrowheads). Representative images were taken along the ventral wall of caudal (hindlimb) regions. At least 3 sections were imaged per sample of 4 or more controls and mutants.